Possible Control of Redox Conditions in the Laser-Heated Diamond Anvil Cell

by

Britany L. Kulka

A Thesis Presented in Partial Fulfillment
of the Requirement for the Degree
Master of Science

Approved April 2021 by the
Graduate Supervisory Committee:

Sang-Heon Shim, Chair
Richard Hervig
Kurt Leinenweber
Thomas Sharp

ARIZONA STATE UNIVERSITY

May 2021

ABSTRACT

The redox conditions of Earth have been changing since proto-Earth's accretion from the solar nebula. These changes have influenced the distribution and partitioning of volatile elements between the atmosphere and the mantle (Righter *et al.*, 2020; Stagno and Fei, 2020). Though oxygen fugacity (fO_2) is arguably not the main factor for phase stability at certain pressure-temperature conditions (McCammon, 2005), it can influence which phases are stable, especially within a closed system such as the ones presented in this study. Despite the importance of controlling fO_2 for interpreting the history of planetary bodies, there have been no methods to control the redox conditions in the laser-heated diamond anvil cell (LHDAC). This thesis has examined the feasibility for controlling redox conditions in the LHDAC using a mixture of Ar and H_2 for insulation media. The experiments of this study were carried out at the GSECARS sector of the Advanced Photon Source at Argonne National Laboratory. In this study, ϵ-FeOOH ($CaCl_2$-type), α-Fe_2O_3 (hematite), and Fe_3O_4 (magnetite) starting materials were used for probing changes of redox conditions. Experiments were also conducted with a pure Ar-medium for ϵ-FeOOH at the same pressure-temperature conditions of the hydrogen-bearing medium in order to provide a reference point for data which has uncontrolled redox conditions for an initially Fe^{2+}-free material. The results for the ϵ-FeOOH starting material in Ar show transformation to ι-Fe_2O_3 (Rh_2O_3(II)-type) at 30.0 GPa and 1900 K, while in Ar + H_2 it transformed to Fe_5O_7 with minor FeH (dhcp) at 30.0 GPa and 1850 K. For α-Fe_2O_3 in Ar + H_2, it was found to convert to ϵ-FeOOH, Fe_5O_7, Fe_5O_6, and FeH (dhcp) at 36.5 GPa and 1800 K. For Fe_3O_4 in Ar + H_2, it was found to convert to Fe_4O_5 ($CaFe_3O_5$-type), Fe_5O_6, and minor FeH (fcc) at 26.0 GPa and 1800 K. These results demonstrate that H in an Ar medium can promote the conversion of some Fe^{3+} to Fe^{2+} and Fe^0. However, the formation of ϵ-FeOOH in the α-Fe_2O_3 starting

material suggests that H may participate in the chemical reaction of iron oxides.

ACKNOWLEDGEMENTS

I would like to thank several people for helping me during my time at ASU including my advisor Sang-Heon Shim, my committee members Thomas Sharp, Kurt Leinenweber, and Richard Hervig, and faculty including but not limited to Edward Garnero, Mingming Li, Arjuin Heimsath, and Christy Till. I would also like to thank members of the geophysics group and my friends at SESE including Byeongkwan Ko, Harrison Allen-Sutter, Helene Piet, Suyu Fu, Claire Richardson, Mara Karageozian, Angelica Berner, Camerian Millsaps, and Qian Yuan.

I would especially like to thank my best friend Jonathan Dolinschi who encouraged me to pursue research which has lead me to obtain this Master's degree and seek a Doctoral position, and for grounding me during difficult times.

I would like to thank the beamline scientists of GSECARS at Argonne National Laboratory, Stella Chariton and Vitali Prakapenka for their help in collecting synchrotron X-ray diffraction, especially during the year 2020. I would also like to thank NASA-Exoplanet, NASA-NExSS, and NSF-EAR for funding this research.

TABLE OF CONTENTS

LIST OF TABLES

Table Page

Table Page

Table Page

LIST OF FIGURES

Figure Page

Figure Page

Figure Page

Figure Page

Chapter 1

INTRODUCTION

Iron oxides are a complex and important component within the Earth's interior (Shim *et al.*, 2009; Dobson and Brodholt, 2005; Tuček *et al.*, 2015) and have proven to have variable stoichiometry (Lavina *et al.*, 2011; Lavina and Meng, 2015; Bykova, 2015; Bykova *et al.*, 2016; Myhill *et al.*, 2016). The complexity of iron oxides is driven by the multivalent element iron (Fe^{3+}, Fe^{2+}, or Fe^{0}), which is the fourth most abundant element in the Earth's mantle. Within a mineral, knowing the valence state of iron allows for a better understanding of the environment it formed in, such as the pressure and temperature where it was stable. Intuitively, it can be said that more oxidized iron, known as ferric iron (Fe^{3+}), would be present in more oxidizing environments such as exposure to water (H_2O or OH). However, there is a paradox to this assumption. McCammon (2005) expanded on this paradox by noting that the structure of the crystal plays an important role in whether ferric iron or ferrous iron (Fe^{2+}) are favorable within a structure at certain pressure and temperature (PT) conditions despite the oxygen fugacity (fO_2). Although fO_2 may not be thought of as an important variable to consider for phase stability, since there can be misconceptions about fO_2 and what exactly it is, fO_2 is likely a variable that will affect the mineral assemblage of rocks, particularly Fe/Mg-bearing silicates (Frost, 1991). A more complete understanding of the Earth's interior requires an understanding of fO_2 with depth and over time, with taking into account what structures are stable at certain PT conditions, what are the available elements, and how much of those elements are available.

Before the Great Oxygenation Event, Earth's atmosphere contained very little

oxygen (O_2) which meant an atmosphere with low fO_2. One possibility is that Earth's accretion from the solar nebula drove differentiation of metals and silicates within the mantle, causing oxygen to redistribute (Righter *et al.*, 2020; Stagno and Fei, 2020). The redistribution within the interior included metallic iron (Fe^0) sinking to the core and the out-gassing of O_2, CO_2, CO, and H_2O vapor into the atmosphere (Righter *et al.*, 2020; Stagno and Fei, 2020). Conditions of the deep interior of the Earth during this redistribution allowed for magma oceans to be present within the interior. These oceans may have began to crystallize once Earth was the size of current-Mars which lead to an increased fO_2 within Earth's lower mantle (Wood *et al.*, 2006). Evidence of this is shown in an Fe^{3+}-rich pyrolitic lower mantle from (Al,Fe)-bearing bridgemantite to have the ratio of Fe^{3+}/Fe^{2+} within the lower mantle of approximately two (Kurnosov *et al.*, 2017). The ferric iron within the lower mantle, however, should be accompanied by a disproportionation reaction such as Eq. 1.1 (Frost *et al.*, 2004; McCammon, 2005).

$$3Fe^{2+} \rightarrow Fe^0 + 2Fe^{3+} \tag{1.1}$$

In experimental mineral physics, the laser-heated diamond anvil cell (LHDAC) has traditionally been used to study minerals with control of the PT conditions of those of planetary interiors. Efforts for redox control have been mainly through the use of redox buffers, such as the fayalite–magnetite oxygen buffer and iron-wüstite buffer, however, these efforts have been mainly for large volume press experiments. Redox buffers differ from the use of a gas medium. Simply put, redox buffers are to buffer the fO_2 of the experiment while the Ar + H_2 medium studied in this research is to ensure reducing conditions. However, redox buffers do allow for the calculation of fO_2, which is what is used in petrology piston-cylinder experiments. Unlike the use of a redox buffer, fO_2 was not able to be calculated for the use of Ar + H_2 medium in this study. The purpose of using Ar + H_2 medium is to ensure sufficiently reducing

conditions within the DAC which is what was done in this study. Although the method presented in this study is more qualitative than quantitative due to current limitations, the use of Ar + H_2 medium ensure reducing conditions within the DAC unlike the use of a redox buffer. This new method also brings a new outlook to experimental DAC setups.

In this study, I contribute to the continuous efforts towards the improvement of experimental redox conditions within the DAC through the use of an Ar + H_2 gas medium. With only 3 vol% H_2, the medium will largely behave as if it is pure argon instead of hydrogen allowing this medium to be safer for gas-loading. This Ar + H_2 medium has been studied with α-Fe_2O_3, ϵ-FeOOH, and Fe_3O_4 within LHDAC. My research has shown that the Ar + H_2 medium promotes the formation of reduced phases compared to those of H_2-free media for α-Fe_2O_3 (Ono *et al.*, 2004), ϵ-FeOOH (this study), and Fe_3O_4 (Ricolleau and Fei, 2016).

Possible Reaction Products					
	Fe^{3+}	Fe^{2+}	Fe^{0}	$Fe^{3+}/\Sigma Fe$	Literature
Fe_2O_3	2	0	0	1	Bykova et al., 2016
Fe_5O_7	4	1	0	0.8	Bykova, 2015
Fe_3O_4	2	1	0	0.67	Bykova, 2015
Fe_4O_5	2	2	0	0.5	Lavina et al., 2011
Fe_5O_6	2	3	0	0.4	Lavina and Meng, 2015
FeO	0	1	0	0	Myhill et al., 2016
FeH	0	0	1	0	Mao et al., 1990

Table 1.1: Possible Reaction Products for Laser-Heated Diamond Anvil Experiments. Column One Lists the Possible Reaction Products from Most Oxidized (Top) to Most Reduced (Bottom). Column Two Shows the Amount of Fe^{3+} in the Respective Product. Column Three Shows the Amount of Fe^{2+} in the Respective Product. Column Four Shows the Amount of Fe^{0} in the Respective Product. Column Five Shows the Amount of Fe^{3+} to the Total Amount of Iron (ΣFe) in the Respective Product. Column Six Cites the Literature Referenced for the Respective Phases (Lavina *et al.*, 2011; Lavina and Meng, 2015; Bykova, 2015; Bykova *et al.*, 2016; Myhill *et al.*, 2016). The Main Take Away Is: The Smaller the Number in Column Five Is, the More Reduced the Product Is. This Is Used to "Measure" The Fe^{3+} : Fe^{2+} Ratio of Products for a Particular Heating Spot.

Chapter 2

MATERIALS AND METHODS

2.1 STARTING MATERIALS

The experiments conducted in this study included three different starting materials α-Fe_2O_3, ϵ-FeOOH, and Fe_3O_4. The purpose of these three starting materials is to study the difference between ferric iron to total iron ratio ($Fe^{3+}/\Sigma Fe$) and the difference between hydrogen-free (α-Fe_2O_3) and hydrogen-bearing (ϵ-FeOOH) starting materials. For varying $Fe^{3+}/\Sigma Fe$ ratio I compared α-Fe_2O_3 which has the ratio of 1, to Fe_3O_4 which has the ratio of 0.67 (Table 2.1). For comparing starting materials with the same $Fe^{3+}/\Sigma Fe$ ratio, I studied α-Fe_2O_3 and ϵ-FeOOH in Ar + H_2 medium. Table 2.1 shows the overview of the three starting materials, the corresponding pressure medium used, and the range of pressure (GPa) and temperature (K) the materials were study at.

Starting Material	Pressure Medium	Pressure Range (GPa)	Temperature Range (K)
Fe_2O_3	$Ar+H_2$	36.5-61.0	1800-1900
FeOOH	$Ar+H_2$	30.0-65.0	1850-1900
	Ar	30.0-52.0	1400-1900
Fe_3O_4	$Ar+H_2$	26.0-35.0	1800-1900

Table 2.1: Overview of All Starting Materials and the Respective Pressure Medium Used with the Range of Pressure and Temperature Conditions Studied. All of the Cells Were Loaded with Both Au and Al_2O_3 in Addition to the Gas Pressure Medium as Pressure Calibrates. The Pressure Error Is $\pm$ 0.5. Temperature Error Is $\pm$100 K Which Is the Typical Minimum Error for Measuring Temperature Using Blackbody Radiation. Heating Spot Information for Each of These Starting Materials Can Be Found in Tables 3.1, 3.2, and 3.3.

2.1.1 ϵ-FeOOH

Starting material ϵ-FeOOH, was synthesized in the 1100-ton, large volume press (LVP) at the Eyring Materials Center at Arizona State University (ASU). For synthesis, the COMPRES 14/8 HT assembly was utilized using a 3 mm diameter Pt capsule and was loaded with a pressed α-Fe_2O_3 pellet (14.8 mg) and 3.3 mg H_2O. The capsule sealed by laser-welding in order to prevent water from escaping the assembly which was confirmed by weighing the capsule before and after welding. The sample was held at 11 GPa and 550 °C for 1 hour with the same approach as Kulka *et al.* (2020). The recovered LVP sample was then sliced axially and the sample was verified as ϵ-FeOOH using the X-ray diffractometer (PANalytical X'Pert PRO MRD) at the Eyring Materials Center at ASU.

For ϵ-FeOOH, the powder was compressed to form a foil $\approx$ 30-50 μm across and 5-10 μm thick. The foil was then placed into a laser-drilled round hole of a pre-indented rhenium gasket on a 200 μm diamond culet using a micromanipulator (Axis Pro SS, Micro Support Co., Ltd., Shizuoka, Japan). The foil was supported by 3-6 spacers of pure ϵ-FeOOH grains ($\leq$5 μm for 200 μm diamond anvil cells (DACs) and $\leq$15 μm for the 400 μm diamond anvil cell(DAC)) on both of the diamond culets. These spacers prevented the foil from coming in contact with the anvils, which reduced thermal conductivity during laser-heating.

Two 200 μm DACs were prepared with ϵ-FeOOH starting material. One 200 μm cell was loaded with pure argon gas (Ar) as the pressure medium and thermal insulator at GeoSoilEnviroCARS (GSECARS) at the Advanced Photon Source (APS). The other 200 μm DAC was loaded with the argon-hydrogen gas containing 3vol% hydrogen (Ar + H_2) as the pressure medium and thermal insulator using the gas loading system (GLS1500, Sanchez Technologies, Frépillon, France) at ASU.

2.1.2 α-Fe_2O_3

For α-Fe_2O_3, the same approach was taken for DAC loading as ϵ-FeOOH. The α-Fe_2O_3 powder was compressed into foil using a symmetric-type DAC utilizing Almax easy Lab type Ia standard design 200 μm diamond anvil cell. One cell was prepared with α-Fe_2O_3. One 200 μm DAC was loaded with the argon-hydrogen gas containing 3vol% hydrogen (Ar+H_2) as the pressure medium and thermal insulator using the gas loading system at ASU.

2.1.3 Fe_3O_4

For Fe_3O_4, the same approach was taken for DAC loading as ϵ-FeOOH and Fe_2O_3. The Fe_3O_4 powder was compressed into foil using a symmetric-type DAC utilizing Almax easy Lab type Ia standard design 400 μm diamond anvil cell. One 400 μm cell was prepared with Fe_3O_4. The cell was loaded with the argon-hydrogen gas containing 3vol% hydrogen (Ar+H_2) as the pressure medium and thermal insulator using the gas loading system at ASU.

2.2 LASER-HEATED DIAMOND ANVIL CELL (LHDAC)

Starting materials were pressed into foils ~40-70 μm wide for 200 μm diamond anvil cells (DACs) and ~150-200 μm wide for 400 μm DACs, and these foils were ~5-10 μm thick. Foils were loaded into laser-drilled round holes in pre-indented rhenium gaskets by hand or utilization of a Microsupport Axis Pro SS micro-manipulator. For each cell, grains of the starting material were used as spacers. For each sample foil, 3-6 spacers were placed on each side of the DAC on the respective culets. Spacers were used for supporting the foil and to reduced heat loss through diamond anvils during laser-heating (Fig. 2.2). Both grains of Au and Al_2O_3 were loaded into the

DACs for pressure calibration. Either pure-Ar or Ar + H_2 gas was loaded to act as a pressure medium and thermal insulator. Pure-Ar gas was loaded at Argonne National Laboratory. The Ar + H_2 gas was loaded using the gas loading system (GLS1500, Sanchez Technologies, Frépillon, France) at ASU. All samples were compressed using a symmetric-type DAC with Almex easyLab type Ia standard design 400 μm diamond anvils (Fig. 2.2).

X-ray diffraction (XRD) was collected *in situ* on the LHDAC experiments using a monochromatic 30 keV or 37 keV X-rays at sector 13-IDD of the GeoSoilEnviroCARS (GSECARS) at the Advanced Photon Source (APS).

Tables 3.1, 3.2, and 3.3 list the LHDAC heating spots for each of the respective DAC setups. The X-ray beam was aligned with the laser-heated spots on the sample foil in the DACs to ensure XRD was collected in the middle of the laser-heated spot. The diameter of the beam used for laser-heating is ~20 μm and for the diameter of the X-ray beam is 5 μm. As long as the alignment of the beams was appropriate, each diffraction pattern represents the iron-phases at the heating temperature. Each heating spot was at least 20 μm away from other heating sports to ensure a pure starting material heating spot. The sample FeOOH under high pressure within a diamond anvil cell can be seen in Fig. 2.3 before laser-heating.

A Dectris Pilatis detector was used to acquire the 2-D diffraction images. These 2-D images were then integrated to 1-D diffraction patterns using the DIOPTAS software (Prescher and Prakapenka, 2015). Diffraction images were collected at 5-15 second exposure before, during, and after heating at high pressure. XRD analysis and phase identification of each phase was done using the software PeakPo (Shim, 2017). Calculated X-ray diffraction peaks based on the unit cell parameters of each of the phases were fit to the observed XRD peaks. The method for determining pressure is to obtain XRD of gold (Au) before heating at pressure because the equation of state

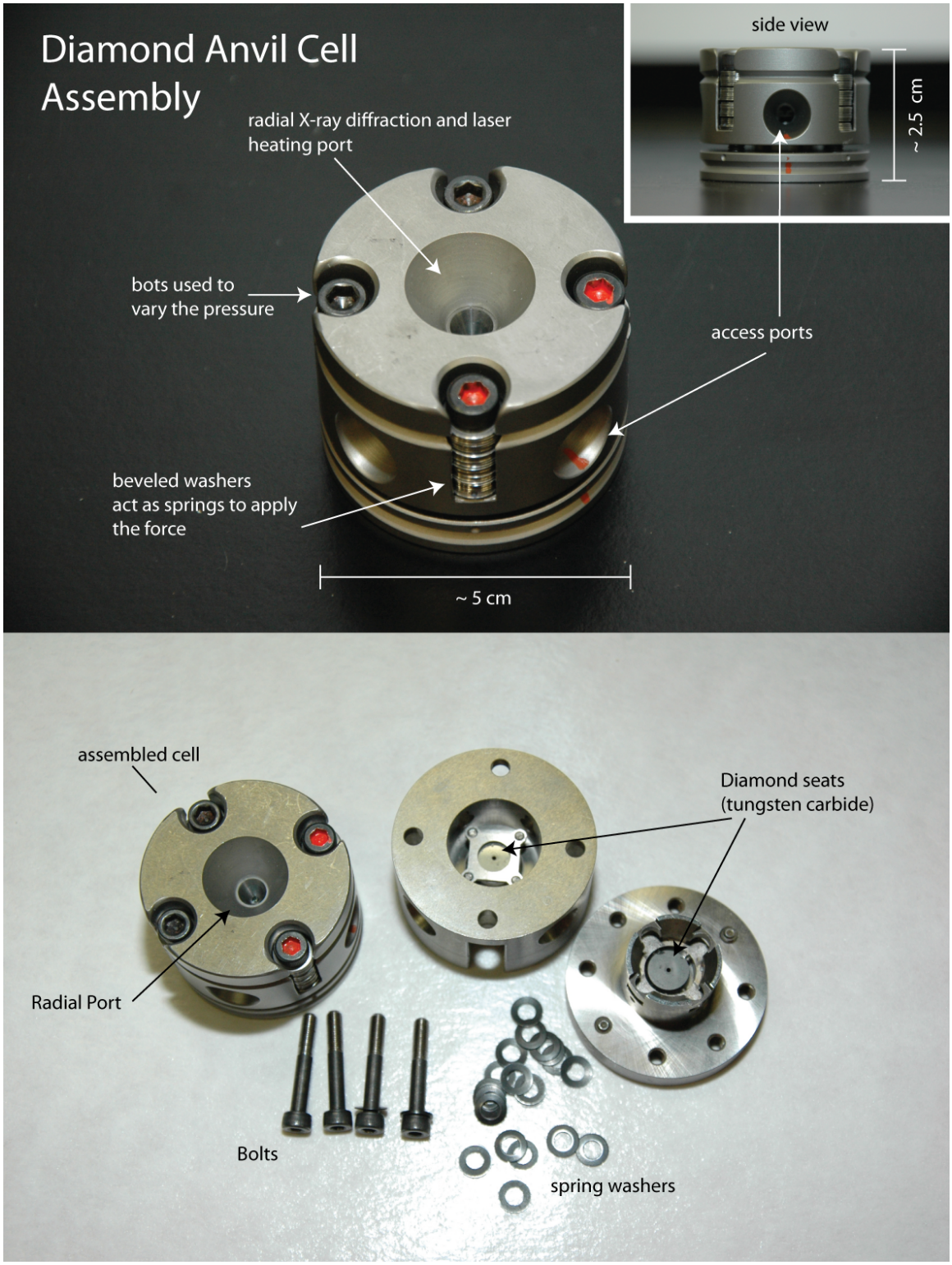

Figure 2.1: Annotate Image of a Diamond Anvil Cell Similar to the Ones Used in This Study. Image Credit: Lavina and Burnley, UNLV

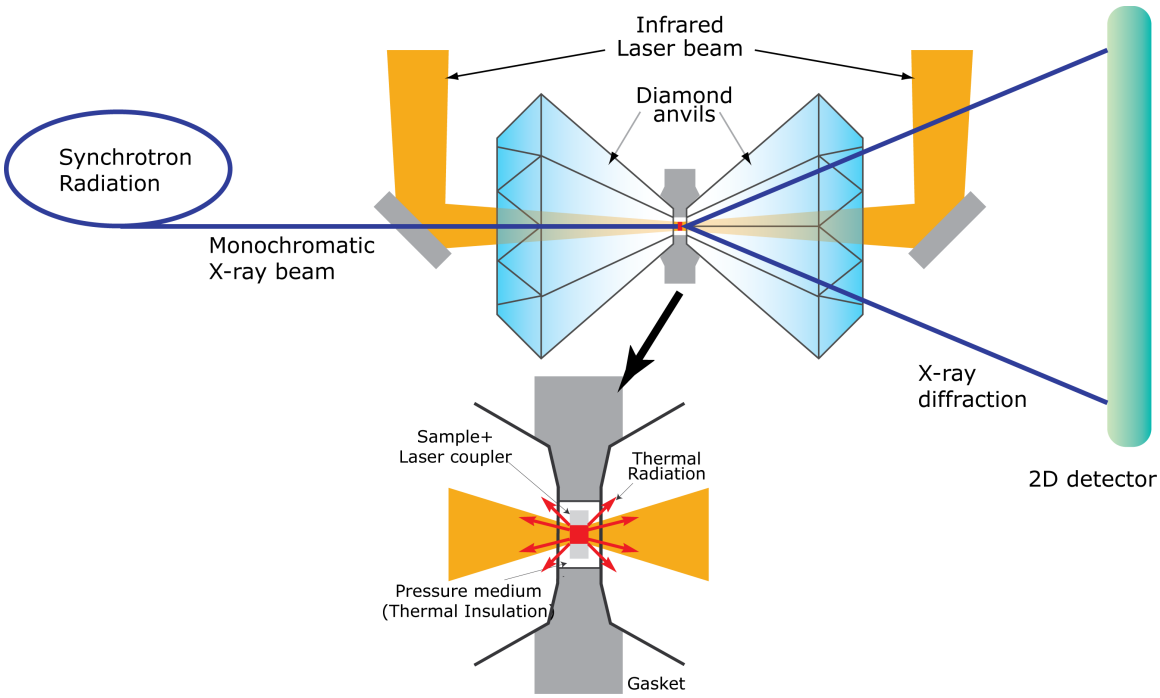

Figure 2.2: Annotated Schematic Diagram Showing X-ray Diffraction on a Diamond Anvil Cell. Image Credit: Sang-Heon Dan Shim, ASU.

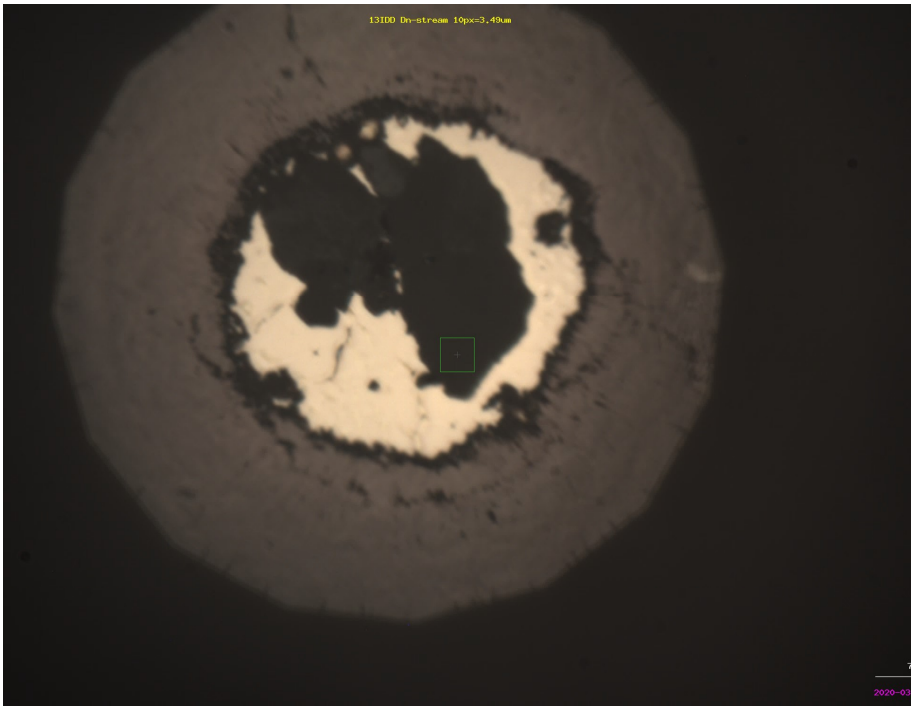

Figure 2.3: Photo of FeOOH Foil in 200 μm DAC at High-Pressure Right Before Laser-Heating.

(Dorogokupets *et al.*, 2015) of Au is well understood. If Au was not found, the Ar peaks were fit in order to determine pressure of the sample chamber during heating using the equation of state (Errandonea *et al.*, 2006).

2.3 X-RAY DIFFRACTION

X-ray diffraction (XRD) is technique used to identify crystalline material by measuring the spacing between the lattice planes. The spacing between the lattice planes within crystalline material are measured in d-spacing (Å).

XRD can be done *ex situ* and *in situ* at the 13-IDD sychrotron beamline. *In situ* XRD which was utilized for this study allowed analysis of phases at high pressure and temperature. For *in situ* XRD, which can be performed at synchrotron facilities using a 2-D detector, a monochromatic X-ray beam is aligned to the sample that is within the diamond anvil cell (DAC) (Fig. 2.2). The beam is then scattered through the lattice planes of the sample causing interaction between the photons and electrons of the material. Angle-dispersive XRD patterns are collected with the 2θ of the 2-D detector. Bragg's law (Eq. 2.1) is used to relate the spacing of the lattice planes with the angle of the X-ray beam.

$$2d \sin\theta = n\lambda \tag{2.1}$$

For Bragg's law (Eq. 2.1), d is the the distance between the lattice planes, θ is the Bragg angle, n is an integer number, and λ is the wavelength of the X-ray beam. For this study, the X-ray beam energies used were 30 keV and 37 keV, which are wavelengths 0.4133 nm and 0.3344 nm, respectively.

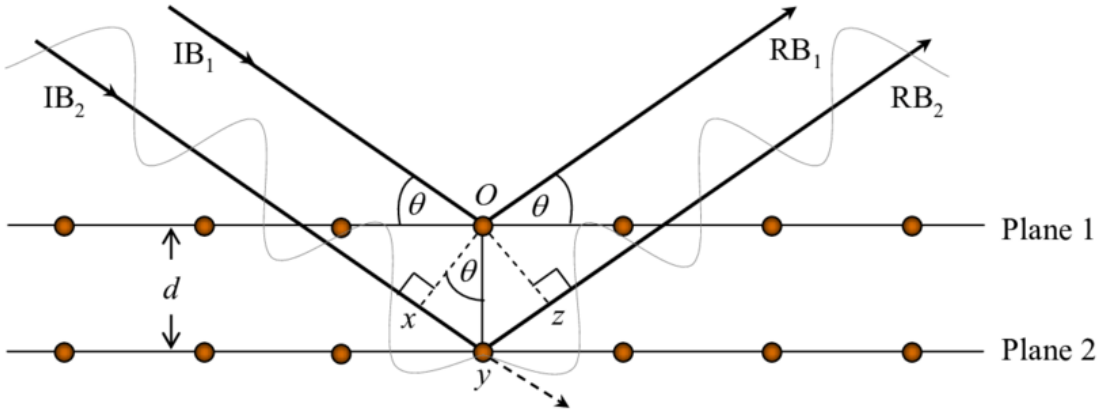

Figure 2.4: Diagram of X-ray Diffraction for Understanding of Bragg's Law 2.1. Plane 1 and Plane 2 Are the Lattice Planes of a Crystal Structure. The Red Circles on the Planes Are Atoms Within the Crystalline Structure. IB_1 and IB_2 Are the Incident X-ray Beam. RB_1 and RB_2 Are the Reflected X-ray Beam. Source: Thomas (2006)

Chapter 3

RESULTS

3.1 LHDAC RESULTS

All three iron oxide starting materials α-Fe_2O_3 (hematite), ϵ-FeOOH ($CaCl_2$-type), and Fe_3O_4 (magnetite) were laser-heated in diamond anvil cells (DACs) at high-pressures and *in situ* XRD was collected. Several reduced iron oxide phases formed during laser-heating in all three starting materials when using the Ar+H_2 pressure medium. Adjustments of 1-10% volume increase and decrease for fitting of the peaks were made with consideration for literature unit-cell volume values at similar pressure and temperature (PT) conditions (Lavina *et al.*, 2011; Lavina and Meng, 2015; Bykova, 2015; Bykova *et al.*, 2016; Myhill *et al.*, 2016).

3.1.1 α-Fe_2O_3

For each chosen heating spot, pre-heating XRD was obtained to ensure that the phase to be heated was only the initial starting material α-Fe_2O_3 (Table 3.1). At spot #1 36.5 GPa and 1800 K, I identified the phases ϵ-FeOOH, Fe_5O_7, Fe_5O_6, and FeH (dhcp) (Fig. 3.1). These phases were also identified for spot #2 48 GPa and 1900 K.

For identification of ϵ-FeOOH, I used the peaks with Miller indices of 110 (d-sp = 3.1453 Å) and $\overline{1}21$ (d-sp = 1.5930 Å). The 110 diffraction peak (d-sp = 3.1453 Å) is the most diagnostic since no other possible phases have peaks at the d-spacing value and this line is the second most intense peak (98% intensity) for ϵ-FeOOH. The 100% intensity line is the 011 peak (d-sp = 2.3475 Å) overlaps with an Ar peak, therefore it was not able to be used for the identification of ϵ-FeOOH. The peak $\overline{1}21$ (d-sp =

1.5930 Å) is 50% the intensity of the most intense peak. The other lines for FeOOH such as the 011 (d-sp = 2.3474 Å) were overlapping with other phases.

For identification of Fe_5O_7 peaks 110 (d-sp = 2.5947 Å) and $20\overline{3}$ (d-sp = 2.5671 Å) were used. The peak $20\overline{3}$ (d-sp = 2.5618 Å) is over a 95% intensity. The peak 110 (d-sp = 2.5947 Å) is about 50% intensity compared with the 100% intensity line which is 202 (d-sp = 2.6266 Å). The 100% intensity line 202 (d-sp = 2.6266 Å) overlaps with an Fe_5O_6 peak (111 (d-sp = 2.6181 Å)), therefore it was not able to be used for the identification of Fe_5O_7.

For identification of Fe_5O_6, peaks 023 (d-sp = 3.4144 Å), 024 (d-sp = 2.8740 Å), 110 (d-sp = 2.6646 Å), and 113 (d-sp = 2.3173 Å) were used. Peaks 023 (d-sp = 3.4144 Å) and 024 (d-sp = 2.8740 Å) are low in intensity (< 20% intensity) but are both diagnostic for the phase Fe_5O_6 due to being low angle peaks (< 8° 2-θ) with no overlapping peaks from other phases. The 100% intensity peak 025 (d-sp = 2.4512 Å) has an overlapping peak for ϵ-FeOOH, therefore was unable to be used for identification. The second and third most intense lines (50% intensity) 133 (d-sp = 1.9352 Å) and 132 (d-sp = 2.0336 Å), respectively, were also unable to be utilized for identification due to over lapping phases. Though peaks at 110 (d-sp = 2.6646 Å) and 113 (d-sp = 2.3173 Å) are less than 35% of the strongest intensity line 025 (d-sp = 2.4512 Å), analysis shows that these peaks align while the unit-cell volume was also considered.

For identification of FeH-dhcp the peaks 004 (d-sp = 1.9892 Å) and 102 (d-sp = 1.8960 Å) were used. The peak 102 (d-sp = 1.8960 Å) is the 100% intensity line. The peak 004 (d-sp = 1.9892 Å) is 40% in intensity. This peak was aligned with spots on the 2-D XRD pattern and makes up the shoulder to the peak at 11.71° 2-θ (d-sp = 2.0246 Å).

At spot #3 61 GPa and 1950 K, I observed ϵ-FeOOH, Fe_5O_7, Fe_5O_6, and FeH-

Sample	Spot #	Medium	Dur. (min)	P Scale	P (GPa)	T (K)	Phase assemblage
Fe_2O_3	1	Ar+H_2	10	Ar	36.5	1800	Fe_5O_6+Fe_5O_7+FeH(dhcp)+FeOOH
Fe_2O_3	2	Ar+H_2	10	Ar	48.0	1900	Fe_5O_6+Fe_5O_7+FeH(dhcp)+FeOOH
Fe_2O_3	3	Ar+H_2	10	Ar	61.0	1950	Fe_5O_6+Fe_5O_7+FeH(dhcp)+FeOOH

Table 3.1: LHDAC Runs for this Study Using Fe_2O_3. All Cells Used Ar as Pressure Calibrant. Each Heating Spot was Heated as a Single Spot with the Maximum Temperature Listed for Each Spot. Temperature Error is ± 100 K. Typically Pressure Increases to Some Degree During Heating. The Pressures Listed are Before Heating and are Not Necessarily Accurate for the Spot During the Heating Cycle.

dhcp during laser-heating. The 1-D XRD patterns of the three heating spots for α-Fe_2O_3 can be seen in Fig. 3.2. For the phases identified, a qualitative analysis of phase fraction can be made based on number of peaks, spots seen on the 2-D XRD pattern and peak intensity. When studying phases present in experiments, the phases Fe_5O_7, ϵ-FeOOH, FeH, and Fe_5O_6 were identified. The certainty in identification varies from least ambiguous to most ambiguous, where the ambiguity relates to number of peaks on the 1-D pattern and spots on the 2-D pattern

For comparison between the effects of the Ar + H_2 and H-free medium have on α-Fe_2O_3, I used the study from Ono *et al.* (2004) which used α-Fe_2O_3 in Ar and NaCl from 12.8-68.2 GPa and 1300-2500 K. Their study identified α-Fe_2O_3 up to 30 GPa, perovskite-type from 30-40 GPa, and post-perovskite-type from 40-70 GPa. These results can be directly compared with my study of α-Fe_2O_3 in the Ar + H_2 pressure medium. All three of these phases identified in Ono *et al.* (2004) only include Fe^{3+} showing that there was no change to the redox conditions. For my study, the phases identified included Fe^{3+}, Fe^{2+}, and Fe^0 which suggests that the hydrogen in the Ar + H_2 pressure medium promoted the reduction of iron unlike a hydrogen-free pressure medium.

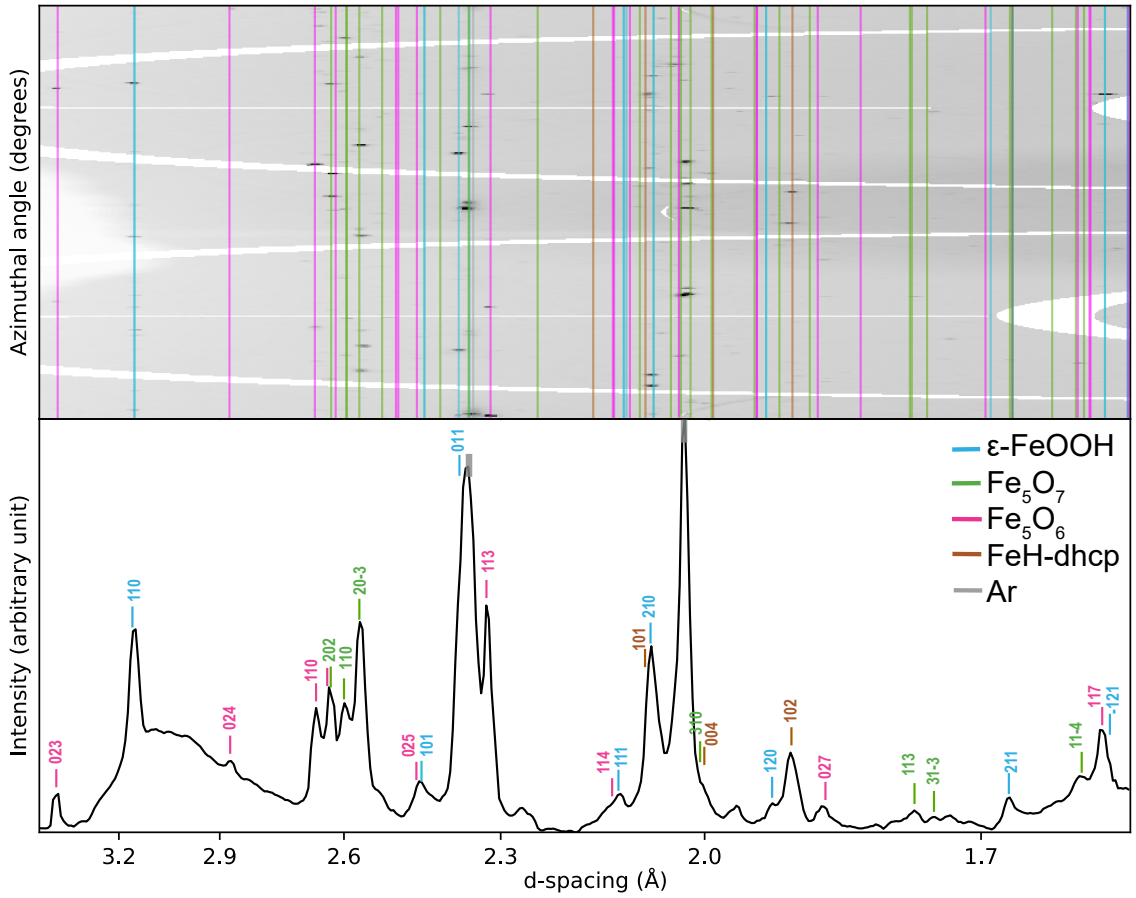

Figure 3.1: *In Situ* X-ray Diffraction (XRD) Pattern (Bottom) 1-D and Unrolled Diffraction Image (Top) 2-D of Starting Material α-Fe_2O_3 at 36.5 GPa and 1800 K in Laser-heated Diamond Anvil Cell (LHDAC). X-ray Energy Was 30 keV. The Vertical Lines in the 2-D Image and Vertical Ticks Show the Expected Peak Positions for the Iron Oxides, Iron Hydroxides, Iron Metal Alloys, and Medium (Ar) for Ar + H_2.

3.1.2 ϵ-FeOOH

XRD was collected before each heating cycle to ensure that there was a spot with the only FeOOH and had not been affected by other laser-heated spots (Table.3.2).

Ar Medium

For starting material ϵ-FeOOH in Ar pressure medium I identified ι-Fe_2O_3 (Rh_2O_3 (II)-type) and ϵ-FeOOH ($CaCl_2$-type) consistently in all four heating spots from 30-

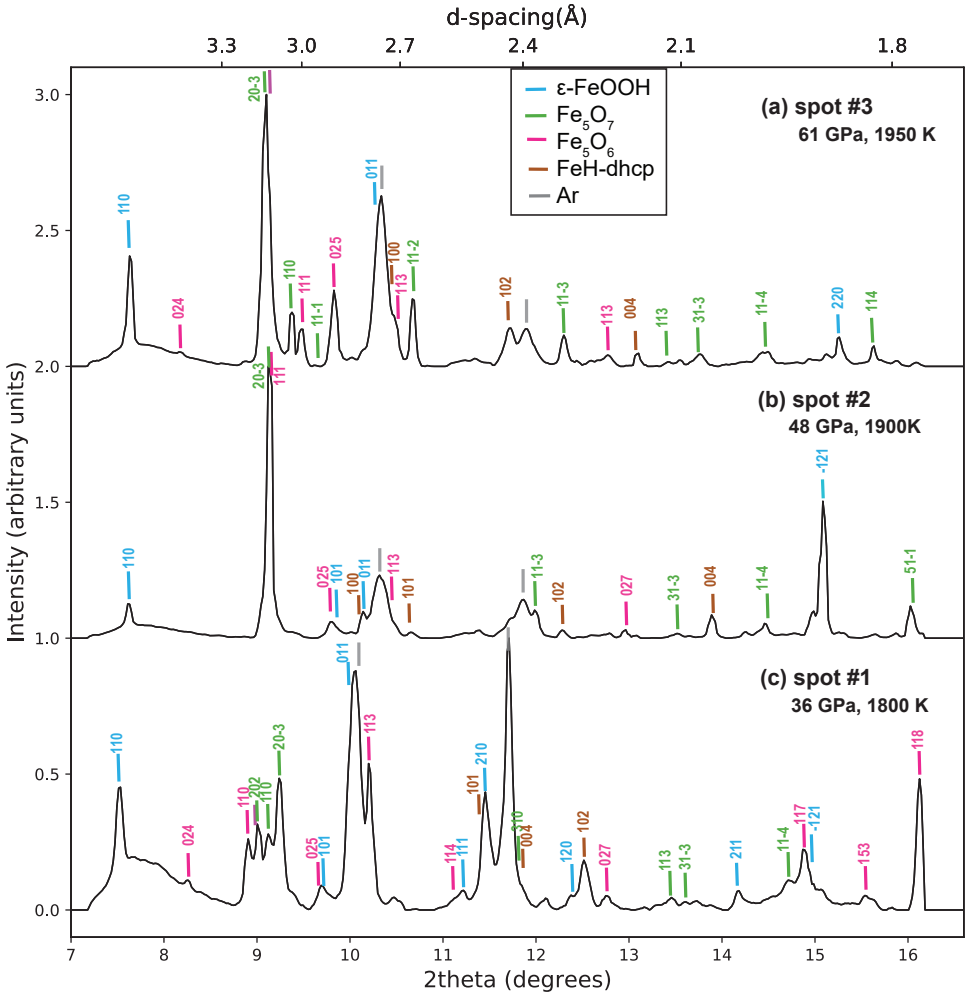

Figure 3.2: *In Situ* X-ray Diffraction (XRD) Patterns of Phases Synthesized from the α-Fe_2O_3 in Ar + H_2 at Different Pressure and Temperature Conditions in the Laser-heated Diamond Anvil Cell (LHDAC). X-ray Energy of 30 keV. The Vertical Ticks Show the Expected Peak Positions for the Iron Oxides, Iron Hydroxides, Iron Metal Alloys, and Medium (Ar) for Ar + H_2. The Corresponding Spot # Has Been Included for Each of the XRD Patterns (Table 3.1).

52 GPa at high-temperatures of 1750-1800 K.

Using XRD for spot #4 at 52 GPa and 1800 K, I identified ι-Fe_2O_3 using peaks 211 (d-sp = 2.5416 Å), 020 (d-sp = 2.5000 Å), 212 (d-sp = 1.8526 Å), and 302 (d-sp = 1.7202 Å) (Fig. 3.3). The 100% intensity line 211 (d-sp = 2.5416 Å) was able to be utilized with no overlapping peaks. Compared with the 100% peak, the peaks 020 (d-sp = 2.5000 Å) is $< 40\%$ intensity, 212 (d-sp = 1.8526 Å) is $> 10\%$ intensity, and 302 (d-sp = 1.7202 Å) is $< 10\%$ intensity. These low intensity ($< 50\%$ intensity) peaks were used for identification of ι-Fe_2O_3 since there were no overlapping phases. Still using XRD for spot #4, I identified ϵ-FeOOH using peaks 110 (d-s = 2.9974 Å) and 020 (d-sp = 1.9909 Å), 220 (d-sp = 1.487 Å). The peak at 2.9974 Å is the second most intense peak ($> 95\%$ intensity) for ϵ-FeOOH. The 100% intense line is 220 (d-sp = 2.2661 Å) and has overlapping peaks with ι-Fe_2O_3 and Ar. The peak 220 (d-sp = 1.487 Å) is less than 50% in intensity when compared to the 100% intensity. The low intensity line is still able to be utilized since there are no overlapping phases. For the phases identified, a qualitative analysis of phase fraction can be made based on number of peaks, spots seen on the 2-D XRD pattern and peak intensity. From most clear phases identified to more ambiguous the phases fluctuate with the most intense depending on the pressure-temperature conditions (Fig. 3.2). The phase ι-Fe_2O_3 is the clearer and more intense phase at spots #1, #2, and #3. However, ϵ-FeOOH is clearer at spot #4. The 2-D XRD in figure 3.3 shows more complete rings made of the the dark spots and narrow peaks in the 1-D image for ϵ-FeOOH, while for ι-Fe_2O_3 the dark spot in the 2-D XRD are more sparse and the peaks in the 1-D are less intense. In figure 3.4 spots #4 and #2 clearly show the the fluctuation between ι-Fe_2O_3 and ϵ-FeOOH. The ϵ-FeOOH peak at $\approx 7.5^\circ$ 2-θ is low in intensity for spot # 2 but is the most intense peak for spot #4 at $\approx 8.0^\circ$ 2-θ. Also, the ι-Fe_2O_3 peak at $\approx 9.0^\circ$ 2-θ is the most intense phase peak for spot #2 but is low in intensity for

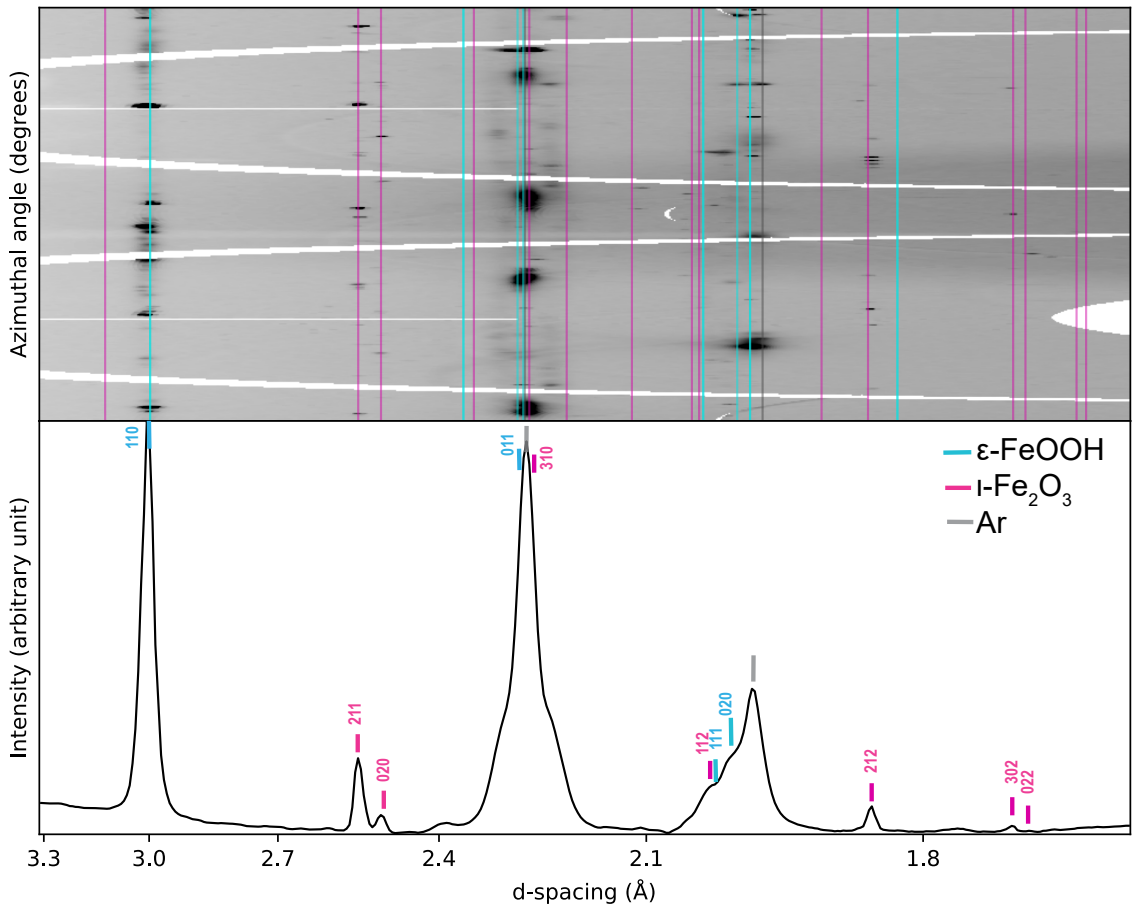

Figure 3.3: *In Situ* X-ray Diffraction (XRD) Pattern (Bottom) 1-D and Unrolled Diffraction Image (Top) 2-D of Starting Material ϵ-FeOOH in Ar at 52 GPa and 1800 K in Laser-heated Diamond Anvil Cell (LHDAC). X-ray Energy Was 30 keV. The Vertical Lines in the 2-D Image and Vertical Ticks Show the Expected Peak Positions for the Iron Oxides, Iron Hydroxides, Iron Metal Alloys, and Pressure Medium (Ar).

spot #4.

Ar + H_2 Medium

For starting material ϵ-FeOOH in an Ar + H_2 medium I identified Fe_5O_7, ϵ-FeOOH, and FeH-dhcp as stable phases in spots #2-5 at 40-65 GPa at high-temperatures of 1850-2400 K. For spot #1 at 30 GPa and 1800 K and spot #6 at 65 GPa and 2400 K, ϵ-FeOOH was not observed. Not observing ϵ-FeOOH at those two spots could be due to complete conversion of the starting material to reaction products owing to

good thermal-insulation at those spots. Reasoning for this is because amongst all the pressure points FeH was identified. The only way for FeH to form from ϵ-FeOOH is through a dehydration reaction. Also at spot #6 65 GPa, the iron oxide phase η-Fe_2O_3 (PPV-type) was identified due to the phase being pressure dependent.

Using XRD for spot #6 at 65 GPa and 2400 K (Fig. 3.5), I identified Fe_5O_7 using peaks 110 (d-sp = 2.6087 Å), 202 (d-sp = 2.5492 Å), $20\overline{3}$ (d-sp = 2.5124 Å), and $31\overline{3}$ (d-sp = 1.7287 Å). The line 202 (d-sp = 2.5492 Å) is the 100% intensity line. The line $20\overline{3}$ (d-sp = 2.5124 Å) is $\approx$ 95% in intensity. The peak 110 (d-sp = 2.6087 Å) is less than 50% the intensity of the 100% line. All lines used for the identification of Fe_5O_7 have no overlapping phases.

Still using spot #6, FeH (dhcp) was identified using peaks 004 (d-sp = 2.0588 Å) and 102 (d-sp = 1.8587 Å). The peak 102 (d-sp = 1.8587 Å) is the 100% intensity line and has no overlapping phases. The 50% intensity line 101 (d-sp = 2.0193 Å) and has overlapping peaks with Fe_5O_7 and η-Fe_2O_3, therefore was unable to be used for identification of FeH (dhcp). For identification of η-Fe_2O_3, the peaks 011 (d-sp = 3.2334 Å), 221 (d-sp = 2.0001 Å), and 012 (d-sp = 1.7125 Å). The line 011 (d-sp = 3.2334 Å) is the 100% intensity line. The line 012 (d-sp = 1.7125 Å) is 95% the intensity of the 100% line. The line 221 (d-sp = 2.0001 Å) is less than 10% of the intensity of the 100% line.

Using XRD of spot #3 for the identification of ϵ-FeOOH, peaks 110 (d-sp = 3.1165 Å) and 011 (d-sp = 2.3368 Å) were used. The line 011 (d-sp = 2.3368 Å) is the 100% intensity line. The line 110 (d-sp = 3.1165 Å) is 95% the intensity of the 100% line.

For the phases identified, a qualitative analysis of phase fraction can be made based on the number of peaks per phase, spots seen on the 2-D XRD pattern and peak intensity. From most clear phases identified to most ambiguous the phases based

on all XRD patterns for this starting material are as follows: Fe_5O_7, FeH (dhcp), ϵ-FeOOH, and η-Fe_2O_3.

This study included experiments using ϵ-FeOOH in both an Ar + H_2 pressure medium mixture and an Ar pressure medium. The Ar + H_2 experiment was at 30-65 GPa and 1850-1900 K, and the Ar experiment was at 30-52 GPa and 1400-1900 K. A direct comparison between the two experiments could be made. For the Ar experiment, phases identified were ι-Fe_2O_3 and ϵ-FeOOH. These phases only include Fe^{3+}. For the Ar + H_2 experiment, phases identified were Fe_5O_7, FeH (dhcp), and ϵ-FeOOH. These identified phases include Fe^{3+}, Fe^{2+}, and Fe^0. The differences between the identified phases in Ar and Ar + H_2 suggests that the Ar + H_2 pressure medium promotes the reduction of iron unlike the hydrogen-free pressure medium.

Sample	Spot #	Medium	Dur. (min)	P Scale	P (GPa)	T (K)	Phase assemblage
FeOOH	1	Ar	10	Au	30.0	1800	ι-Fe_2O_3+FeOOH
FeOOH	2	Ar	12	Au	40.0	1750	ι-Fe_2O_3+FeOOH
FeOOH	3	Ar	10	Au	46.0	1800	ι-Fe_2O_3+FeOOH
FeOOH	4	Ar	11	Au	52.0	1800	ι-Fe_2O_3+FeOOH
FeOOH	1	Ar+H_2	10	Au	30.0	1850	Fe_5O_7+FeH(dhcp)+FeOOH
FeOOH	2	Ar+H_2	10	Au	40.0	1850	Fe_5O_7+FeH(dhcp)+FeOOH
FeOOH	3	Ar+H_2	11	Au	46.0	1950	Fe_5O_7+FeH(dhcp)+FeOOH
FeOOH	4	Ar+H_2	12	Au	50.0	1900	Fe_5O_7+FeH(dhcp)+FeOOH
FeOOH	5	Ar+H_2	10	Au	60.5	1900	Fe_5O_7+FeH(dhcp)+FeOOH
FeOOH	6	Ar+H_2	10	Au	65.0	2400	Fe_5O_7+FeH(dhcp)+FeOOH+η-Fe_2O_3

Table 3.2: LHDAC Runs for This Study Using ϵ-FeOOH. All Cells Used Au And/Or Ar as Pressure Calibrant. Each Heating Spot Was Heated as a Single Spot with the Maximum Temperature Listed for Each Spot. Temperature Error Is ± 100 K. Pressure Increases to Some Degree During Heating. The Pressure Listed in the Table Is the Pressure Before Heating.

3.1.3 Fe_3O_4

For starting material Fe_3O_4 (magnetite) in the Ar + H_2 medium I identified Fe_4O_5 ($CaFe_3O_5$-type), Fe_5O_6, and FeH (fcc) from 26-35 GPa at high-temperatures

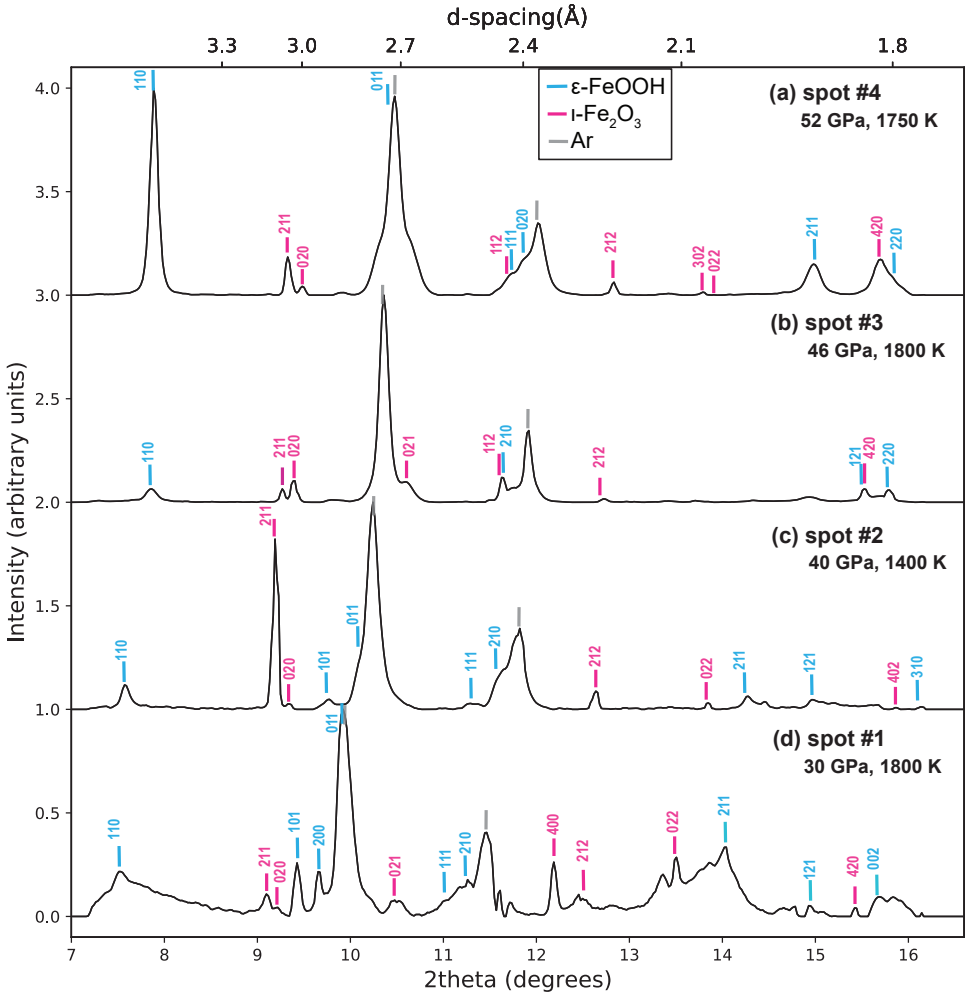

Figure 3.4: *In Situ* X-ray Diffraction (XRD) Patterns of Phases Synthesized from the ϵ-FeOOH in Ar at Different Pressure and Temperature Conditions in the Laser-heated Diamond Anvil Cell (LHDAC). X-ray Energy of 30 keV. The Vertical Ticks Show the Expected Peak Positions for the Iron Oxides, Iron Hydroxides, Iron Metal Alloys, and Pressure Medium (Ar). The Corresponding Spot # Has Been Included for Each of the XRD Patterns (Table 3.2).

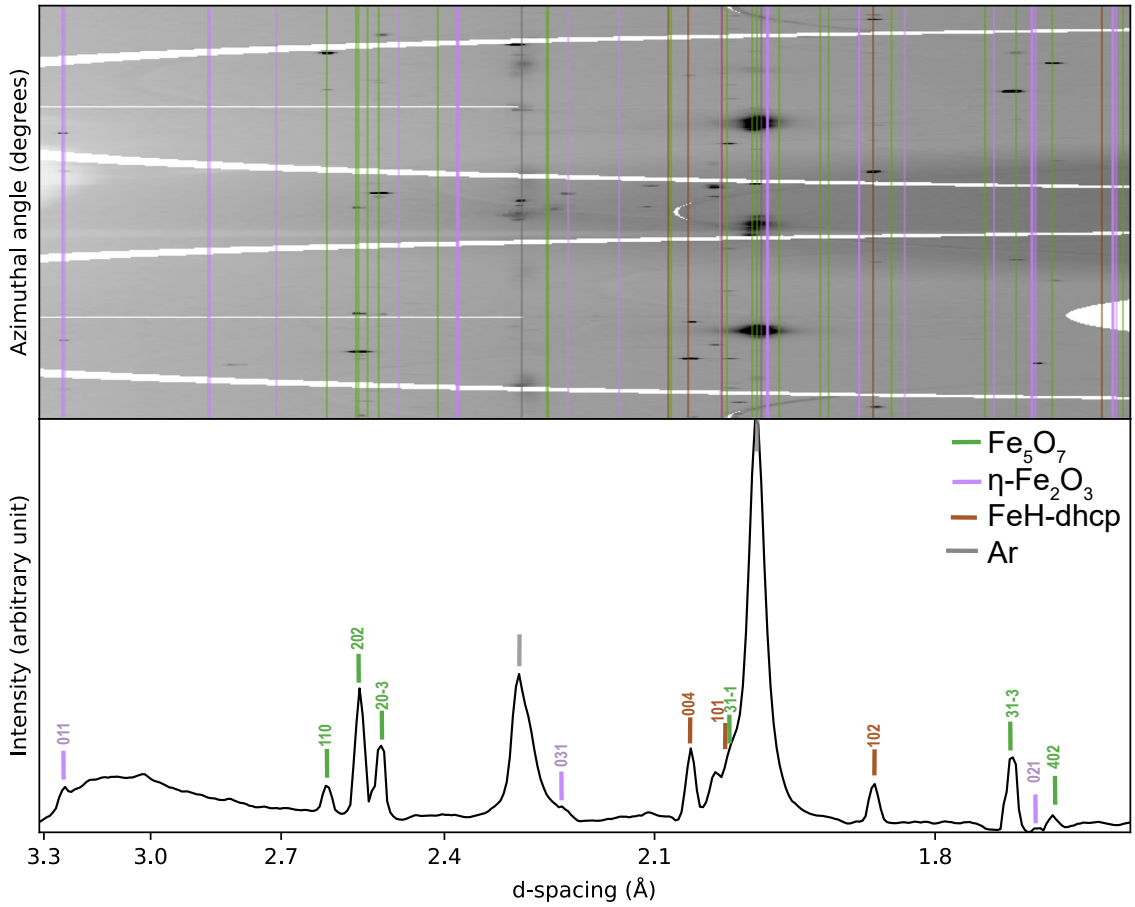

Figure 3.5: *In Situ* X-ray Diffraction (XRD) Pattern (Bottom) 1-D and Unrolled Diffraction Image (Top) 2-D of Starting Material ϵ-FeOOH in Ar + H_2 at 65 GPa and 2400 K in Laser-heated Diamond Anvil Cell (LHDAC). X-ray Energy Was 30 keV. The Vertical Lines in the 2-D Image and Vertical Ticks Show the Expected Peak Positions for the Iron Oxides, Iron Hydroxides, Iron Metal Alloys, and Pressure Medium (Ar).

of 1800-1900 K.

Using XRD for spot #3 at 35 GPa and 1800 K (Fig. 3.7), the identification of Fe_4O_5 peaks 024 (d-sp = 2.5904 Å), 130 (d-sp = 2.1207 Å), 131 (d-sp = 2.0901 Å), 026 (d-sp = 1.8895 Å), 115 (d-sp = 1.8323 Å), and 008 (d-sp = 1.5441 Å) were used. The peak 024 (d-sp = 2.5904 Å) is the 100% intensity line and has no overlapping phases. Peaks 130 (d-sp = 2.1207 Å), 131 (d-sp = 2.0901 Å), 026 (d-sp = 1.8895 Å), 115 (d-sp = 1.8323 Å), and 008 (d-sp = 1.5441 Å) are all less than 50% the intensity of the 100% peak, however, all have no overlapping peaks. For identification of Fe_5O_6,

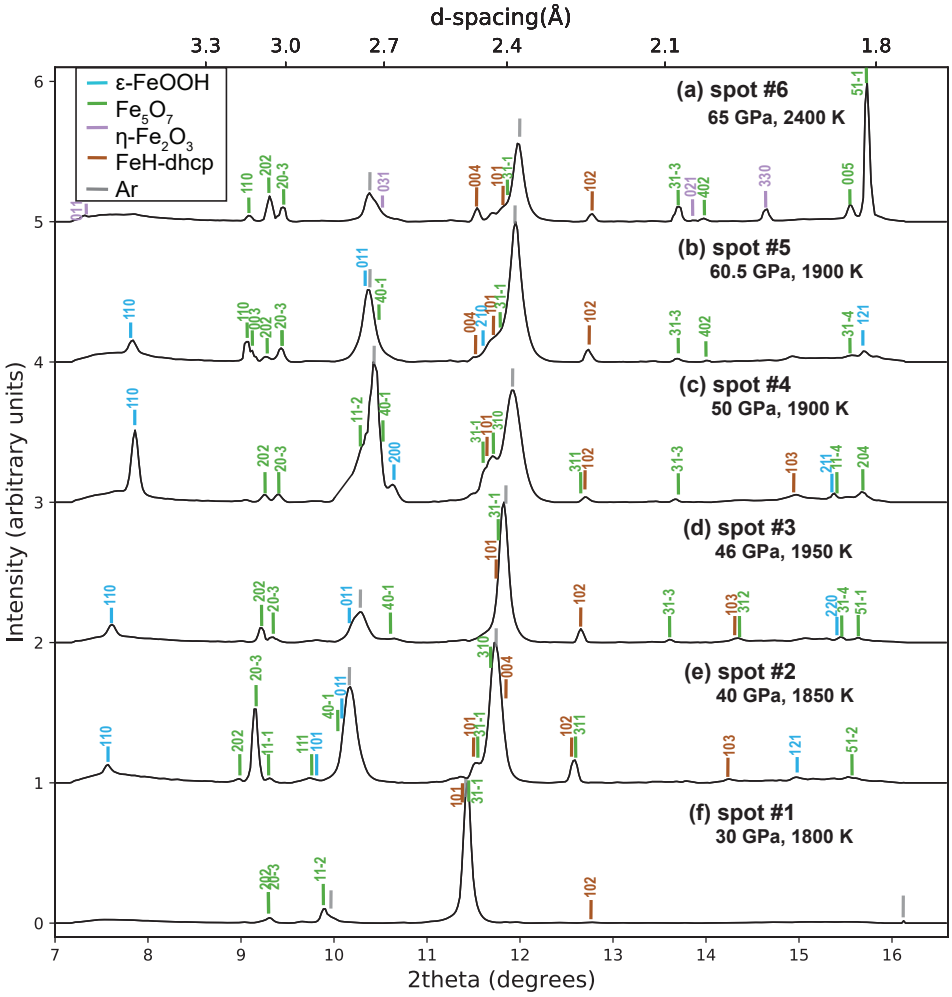

Figure 3.6: *In Situ* X-ray Diffraction (XRD) Patterns of Phases Synthesized from the ϵ-FeOOH in Ar + H_2 at Different Pressure and Temperature Conditions in the Laser-heated Diamond Anvil Cell (LHDAC). X-ray Energy of 30 keV. The Vertical Ticks Show the Expected Peak Positions for the Iron Oxides, Iron Hydroxides, Iron Metal Alloys, and Pressure Medium (Ar). The Corresponding Spot # Has Been Included for Each of the XRD Patterns (Table 3.2).

peaks 112 (d-sp = 2.5546 Å), 025 (d-sp = 2.5236 Å), 1.9818 Å, 027 (d-sp = 1.9556 Å), 133 (d-sp = 1.9195 Å), 135 (d-sp = 1.7123 Å), 046 (d-sp = 1.5568 Å), 137 (d-sp = 1.4982 Å) and 138 (d-sp = 1.3807 Å) were used. The 100% intensity line at 2.5211 Å has no overlapping phases and many (> 5) dark spots on the 2-D XRD (Fig. 3.7). The 95% intensity line is at 1.9818 Å. This peak is low and unclear but there are more than ten spots on the 2-D XRD pattern. The lines at 112 (d-sp = 2.5546 Å), 027 (d-sp = 1.9556 Å), 133 (d-sp = 1.9195 Å), 135 (d-sp = 1.7123 Å), 046 (d-sp = 1.5568 Å), 137 (d-sp = 1.4982 Å), and 138 (d-sp = 1.3807 Å) are less than 50% in intensity compared to the 100% line. These low intensity lines are accompanied by both low intensity peaks and few spots on the 2-D XRD pattern. For identification of FeH (fcc), peaks 111 (d-sp = 2.0481 Å) and 200 (d-sp = 1.7737 Å).

For the phases identified, a qualitative analysis of phase fraction can be made based on the number of peaks per phase, spots seen on the 2-D XRD pattern and peak intensity. From most clear phases identified to most ambiguous the phases based on all XRD patterns for this starting material are as follows: Fe_4O_5, Fe_5O_6, and FeH (fcc).

For comparison between the effects of the Ar + H_2 and H-free medium have on Fe_3O_4, I used the study from Ricolleau and Fei (2016) which used Fe_3O_4 in Ar and Ne from 26-64 GPa and 1300-2300 K. Their study identified h-Fe_3O_4. This identified phases has the same iron valence state as the starting material which suggest that there was no change in redox conditions. These results can be directly compared with my study of Fe_3O_4 in the Ar + H_2 pressure medium. For my study, the phases identified included Fe_4O_5, Fe_5O_6, and FeH (fcc). These identified phases include iron at valence states of Fe^{3+}, Fe^{2+}, and Fe^0. This suggests that the hydrogen in the Ar + H_2 pressure medium promoted the reduction of iron unlike a hydrogen-free pressure medium in Ricolleau and Fei (2016).

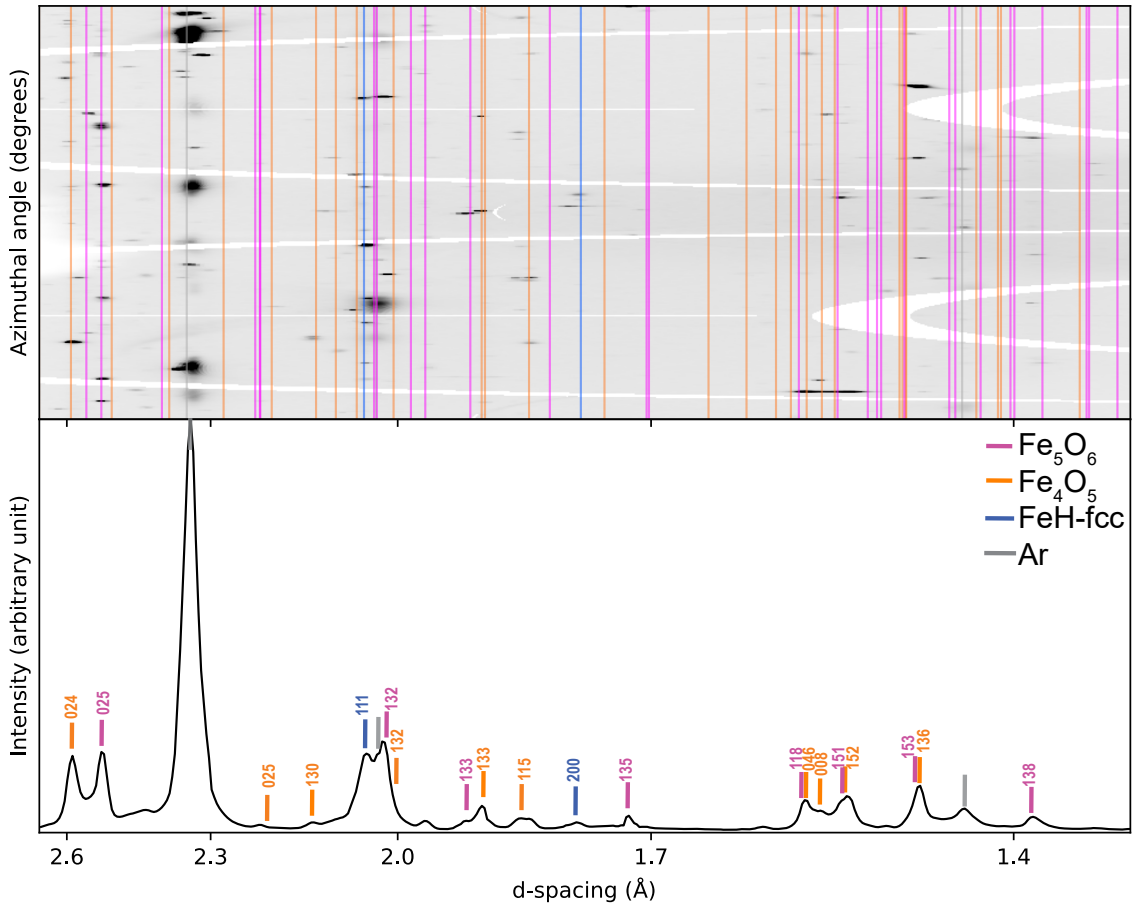

Figure 3.7: *In situ* X-ray Diffraction (XRD) Pattern (bottom) 1-D and Unrolled Diffraction Image (Top) 2-D of Starting Material Fe_3O_4 at 35 GPa and 1800 K in Laser-Heated Diamond Anvil Cell (LHDAC). X-ray Energy was 37 keV. The Vertical Lines in the 2-D Image and Vertical Ticks show the Expected Peak Positions for the Iron Oxides, Iron Hydroxides, Iron Metal Alloys, and Pressure Medium (Ar).

Sample	Spot #	Medium	Dur. (min)	P Scale	P (GPa)	T (K)	Phase assemblage
Fe_3O_4	1	Ar+H_2	10	Ar	26.0	1800	Fe_4O_5+Fe_5O_6+FeH(fcc)
Fe_3O_4	2	Ar+H_2	8	Ar	30.0	1900	Fe_4O_5+Fe_5O_6+FeH(fcc)
Fe_3O_4	3	Ar+H_2	9	Ar	35.0	1800	Fe_4O_5+Fe_5O_6+FeH(fcc)

Table 3.3: Laser-Heated Diamond Anvil Cell (LHDAC) Runs for This Study Using Fe_3O_4. All Cells Used Au And/Or Ar as Pressure Calibrant. Each Heating Spot Was Heated as a Single Spot with the Maximum Temperature Listed for Each Spot. Temperature Error Is ± 100 K. Pressure Increases to Some Degree During Heating. The Pressure Listed in the Table is the Pressure Before Heating.

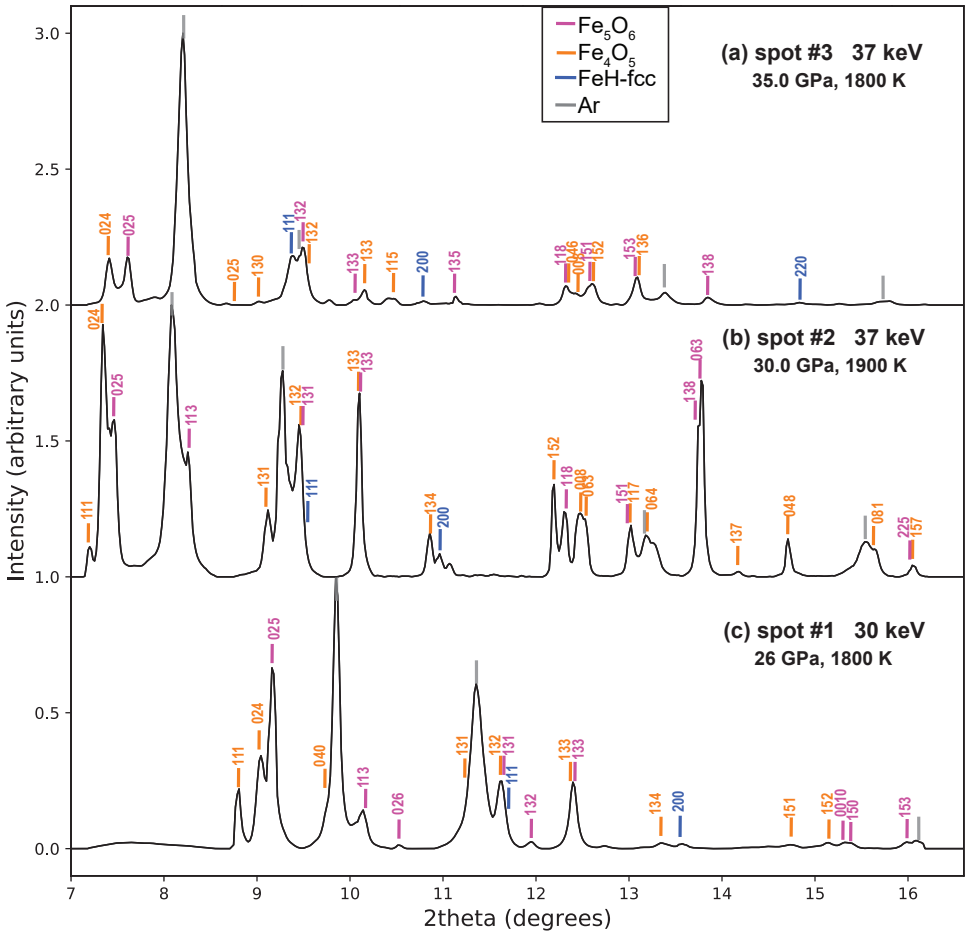

Figure 3.8: *In Situ* X-ray Diffraction (XRD) Patterns of Phases Synthesized from the Fe_3O_4 Starting Material at Different Pressure and Temperature Conditions in the Laser-Heated Diamond Anvil Cell (LHDAC) with X-ray Energy of (a),(b) 37 keV for 30 and 35 GPa, and (c) 30 keV for 26 GPa. The Vertical Ticks Show the Expected Peak Positions for the Iron Oxides, Iron Hydroxides, Iron Metal Alloys, and Pressure Medium (Ar). The Corresponding Spot # has been Included for Each of the XRD Patterns (Table 3.3).

Chapter 4

DISCUSSION

4.1 GIBBS' PHASE RULE

To better understand the phases that were identified from XRD analysis, I referred to Gibbs' Phase Rule (Eq. 4.1). Gibbs' Phase Rule applies to closed homogeneous systems under thermodynamic equilibrium. However, because laser-heating the sample is done as spots and not the whole sample at once, it is not technically a closed system since there can be interaction between the heated spot and the non-heated sample it is surrounded by (Fig. 4.1). The heated spot also has a thermal gradient which can mean that if the laser for heating and the X-ray beam are not perfectly aligned, then there is a possibility that not all the phases that can be identified in XRD may be equilibrium phases. Other reasons that Gibbs' Rule is not fully applicable with regards to the laser-heated spots not being part of a closed system also include the experiments would likely be affected by heterogeneities in pressure, temperature, and composition, and it is also important to consider kinetic effects. Nevertheless, Gibbs' Rule can be useful for identifying the phases which form under equilibrium conditions in the experiments. The Gibbs' Phase Rule has three components, F: degrees of freedom, C: number of components, and Φ: number of phases.

$$F = C - \Phi + 2 \tag{4.1}$$

For this study, each experiment had two degrees of freedom that were controlled, temperature and pressure, so F = 2. The other variables for this equation will be explained for each of the starting materials within the respective sections.

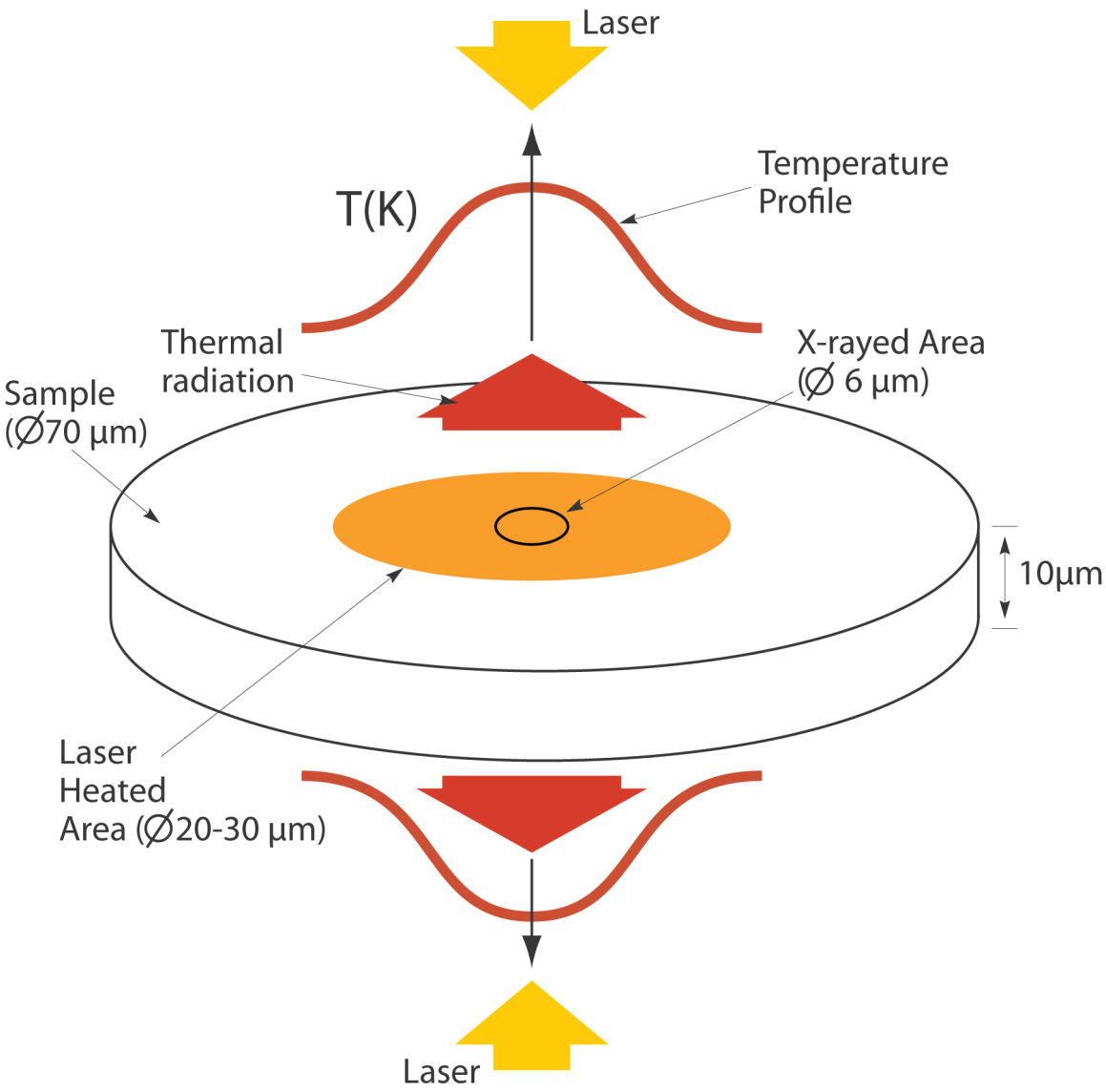

Figure 4.1: Diagram of Sample During Laser-Heating Showing the Spot for Heating and Spot for XRD are Different in Size, and That The Heating Spot has a Thermal Gradient. If the Laser for Heating and X-ray Beam are Misaligned, the XRD Collected Would not be at the Center of the Heating Spot. Lower Temperature Spots Would Mean that Not All of the Phases Identified in XRD may not be in Equilibrium. Source: Sang-Heon Dan Shim, ASU.

4.1.1 Ar + H_2 MEDIUM AS A REDUCING AGENT

Looking at the phases produced during laser-heating at high pressure allows for the interpretation that Ar + H_2 pressure medium mixture creates a reducing envi-

ronment that promotes reduced forms of iron (Fe^{2+} and Fe^0). The starting materials α-Fe_2O_3 (hematite), ϵ-FeOOH ($CaCl_2$-type), and Fe_3O_4 (magnetite) were all studied within the Ar + H_2 medium mixture. This study using Ar + H_2 has been directly compared with hydrogen-free medium from this study and literature (Ono *et al.*, 2004; Ricolleau and Fei, 2016). The use of Ar + H_2 suggests that this method promotes reduced iron oxide phases to form based on XRD analysis.

α-Fe_2O_3 in Ar + H_2 Medium

For experiments with Fe_2O_3 in the Ar + H_2 pressure medium, phases I identified Fe_5O_7, Fe_5O_6, FeH (dhcp), and ϵ-FeOOH from *in situ* XRD patterns from laser-heating at 36.5-61 GPa and 1800-1900 K. (Eq. 4.2).

$$7Fe_2O_3 + 2H_2 \rightarrow Fe_5O_7 + Fe_5O_6 + 4FeH + 4O_2 \tag{4.2}$$

$$O_2 + 2H_2 \rightarrow 2H_2O \tag{4.3}$$

$$Fe_2O_3 + H_2O \rightarrow 2FeOOH \tag{4.4}$$

Using Gibbs' Phase Rule (Eq. 4.1), the number of products for this reaction are able to be checked. In the experiment for Fe_2O_3, there were 2 degrees of freedom (F) which were pressure and temperature, and there were 3 components (C) which were Fe, O, and H. These numbers can be put into Gibbs' Rule to find Φ (Eq. 4.5).

$$2 = 3 - \Phi + 2 \tag{4.5}$$

Following Gibbs' Phase Rule, it is found that Φ should be 3. There were four products identified from XRD analysis as mentioned above, Fe_5O_7, Fe_5O_6, FeH (dhcp), and ϵ-FeOOH. In the initial reaction between Fe_2O_3 and H_2 (Eq. 4.2), O_2 (or H_2O) was released from the reaction. The O_2 that is released then reacts with the H_2 within the starting material to form H_2O (Eq. 4.3). The H_2O is then able to react with

Fe_2O_3 that is outside of the heating spot (Eq. 4.4). Therefore, ϵ-FeOOH is metastable relative to the other three products and is not part of the of the equilibrium reaction at the laser-heated spot. FeH was also identified using XRD. The hydrogen amount in FeH fluctuates and there is no correlation with pressure (Table 4.1).

Fe_5O_7 has the most intense peaks in the XRD (Fig. 3.2). Fe_5O_7 is also seen in the ϵ-FeOOH experiments which is similar to Fe_2O_3 because both starting materials only have Fe^{3+}. For Φ to equal 3, the products from the thermodynamically stable reaction are are Fe_5O_7, FeH, and O_2 (Fig. 4.2). This leaves Fe_5O_6 as the other metastable phase. Within XRD, the phase Fe_5O_6 showed the most fluctuation in terms of peak intensity in the 1-D XRD and number of clear spots on the 2-D XRD which leads the conclusion that if Gibbs' Rule must be met, then Fe_5O_6 is unlikely a stable phase. With that said, the metastability of Fe_5O_6 may due to factors such as the thermal and stress gradients which can result in local disequilibrium within the heated spot. In the XRD for Fe_2O_3, Fe_5O_6 was seen in all diffraction patterns, however, the peaks fluctuate with pressure (Fig. 3.2). This can be seen for instance when referring to the peaks at $\approx 8.3^\circ$ 2-θ. For the XRD of spot #1 which was collected at 36 GPa and 1800 K, peak is low in intensity compared to the peaks of other phase but is there. When increasing pressure, for spot # 2 collected at 48 GPa and 1900 K, the peak at $\approx 8.3^\circ$ 2-θ is no longer there. Lastly, for spot # 3 collected at 61 GPa and 1950 K, the peak at $\approx 8.3^\circ$ 2-θ appears though it is still low in intensity compared to the other peaks in the same XRD.

ϵ-FeOOH in Ar + H_2 Medium

For experiments with ϵ-FeOOH in the Ar + H_2 pressure medium, I identified Fe_5O_7 and FeH(dhcp) from *in situ* XRD patterns from laser-heating at 30-65 GPa and 1850-1900 K (Eq. 4.6). Analysis of XRD showed that the starting material ϵ-FeOOH was

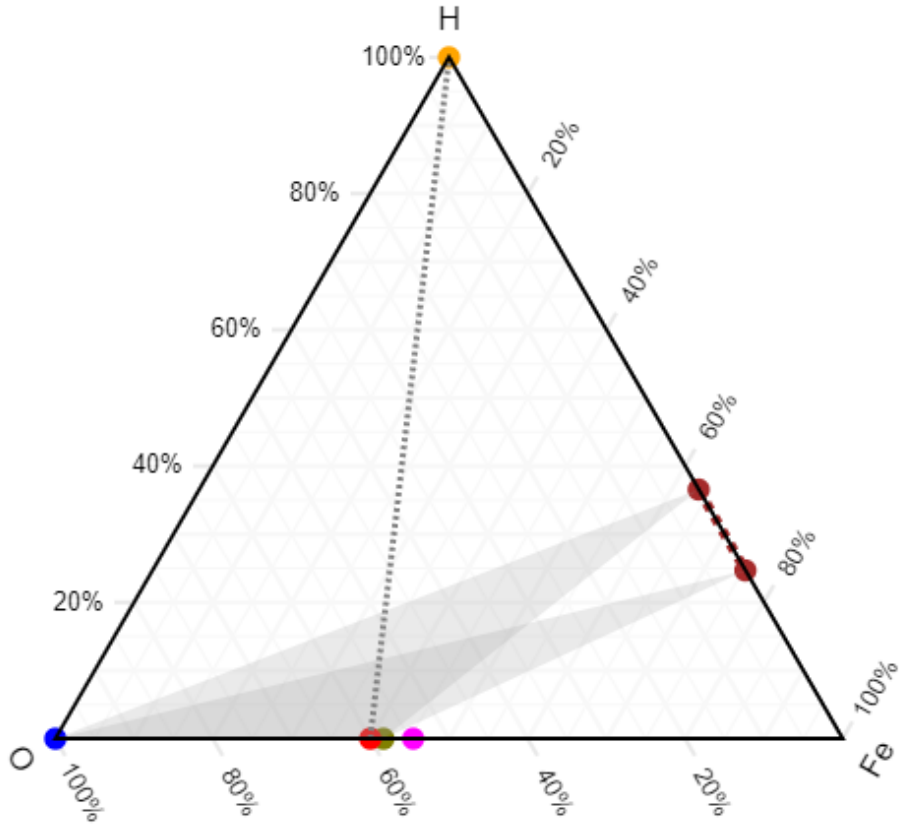

Figure 4.2: Ternary Diagram for α-Fe_2O_3 in Ar + H_2. Circles are of Phases Fe_2O_3: Red, Fe_5O_7: Green, Fe_5O_6: Magenta, O_2: Blue, FeH: Brown, and H_2: Orange. The Grey Dotted Line Connects the Reactants; Fe_2O_3 and H_2. The Brown Dashed Line Connect the Minimum and Maximum Calculated Hydrogen Amounts in FeH (Table 4.1). The Grey Areas Connect the Stable Products; Fe_5O_7, FeH_x, and H_2O.

still observable.

$$13FeOOH + 7H_2 \rightarrow 2Fe_5O_7 + 3FeH + 12H_2O \tag{4.6}$$

Using Gibbs' Phase Rule (Eq. 4.1), the number of products for this reaction are able to be checked. In the experiment for ϵ-FeOOH, there were 2 degrees of freedom (F) which were pressure and temperature, and there were 3 components (C) which were Fe, O, and H. These numbers can be put into Gibbs' Rule to find Φ (Eq. 4.7).

$$2 = 3 - \Phi + 2 \tag{4.7}$$

Following Gibbs' Phase Rule, it is found that Φ should be 3. Referring to Eq. 4.6, there are three phases. H_2O is a product which is from the dehydration reaction. The ϵ-FeOOH that could be observed in *in situ* XRD is non-reacted starting material. The hydrogen amount in the FeH fluctuates and there is no correlation with pressure (Table. 4.1). Also similar to the Fe_2O_3, the phase Fe_5O_7 has the most intense peaks in the XRD (Fig. 3.6). Therefore, Gibbs' Phase Rule requirement is met and with the stable phases being Fe_5O_7, FeH, and H_2O (Fig. 4.3).

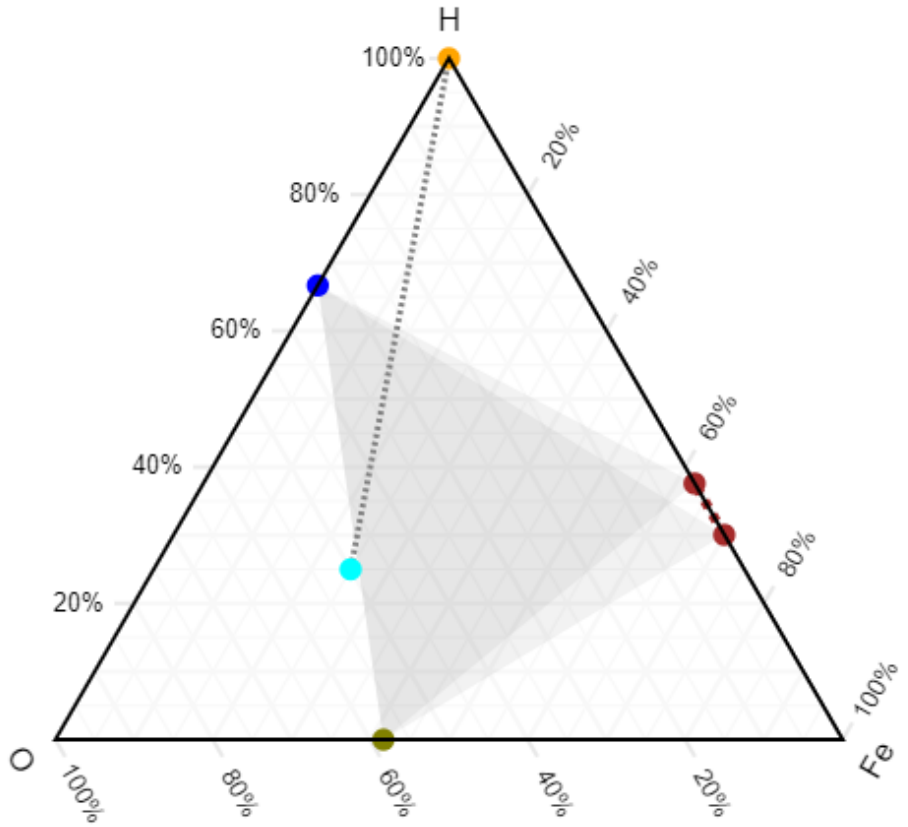

Figure 4.3: Ternary Diagram for FeOOH in Ar + H_2. Circles Are of Phases ϵ-FeOOH: Cyan, Fe_5O_7: Green, H_2O: Blue, FeH: Brown, and H_2: Orange. The Brown Dashed Line Connect the Minimum and Maximum Calculated Hydrogen Amounts in FeH (Table 4.1). The Grey Dotted Line Connects the Reactants; ϵ-FeOOH and H_2. The Grey Areas Connect the Stable Products; Fe_5O_7, FeH_x, and H_2O.

Fe_3O_4 in Ar + H_2 Medium

For experiments with Fe_3O_4 in Ar + H_2 pressure medium, I identified Fe_4O_5, Fe_5O_6, and FeH (fcc) from *in situ* XRD patterns from laser-heating at 26-35 GPa and 1800-1900 K (Eq. 4.8).

$$5Fe_3O_4 + H_2 \rightarrow 2Fe_4O_5 + Fe_5O_6 + 2FeH + 2O_2 \tag{4.8}$$

Using Gibbs' Phase Rule (Eq. 4.1), the number of products for this reaction are able to be checked. In the experiment for Fe_3O_4, there were 2 degrees of freedom (F) which were pressure and temperature, and there were 3 components (C) which were Fe, O, and H. There numbers can be put into Gibbs' Rule to find Φ (Eq. 4.9).

$$2 = 3 - \Phi + 2 \tag{4.9}$$

Following Gibbs' Phase Rule, it is found that Φ should be 3. Referring to Eq. 4.8, there are four products, not three. Fe_4O_5 and Fe_5O_6 were identified using *in situ* XRD and are stable products (Fig. 3.8). In the reaction, O_2 is a product which is a required product for the redox reaction. The XRD showed FeH peaks that were fluctuating and low in intensity for each of the pressures (Fig. 3.8). There is uncertainty about what the thermodynamically stable phases are, however, similarly to the approach used regarding the identification of Fe_5O_6 for the Fe_2O_3 experiments, peak intensity in the 1-D XRD and number of clear spots on the 2-D can be examined. The least clear phase in XRD was Fe_5O_6 which would bring the conclusion that Fe_5O_6 unlikely a stable phase. The metastability of Fe_5O_6 may due to factors such as the thermal and stress gradients which can result in local disequilibrium within the heated spot. Through this conclusion, it is interpreted that the thermodynamically stable phases would be Fe_4O_5, FeH, and O_2 (Fig. 4.4) and that Fe_5O_6 would be the metastable phase.

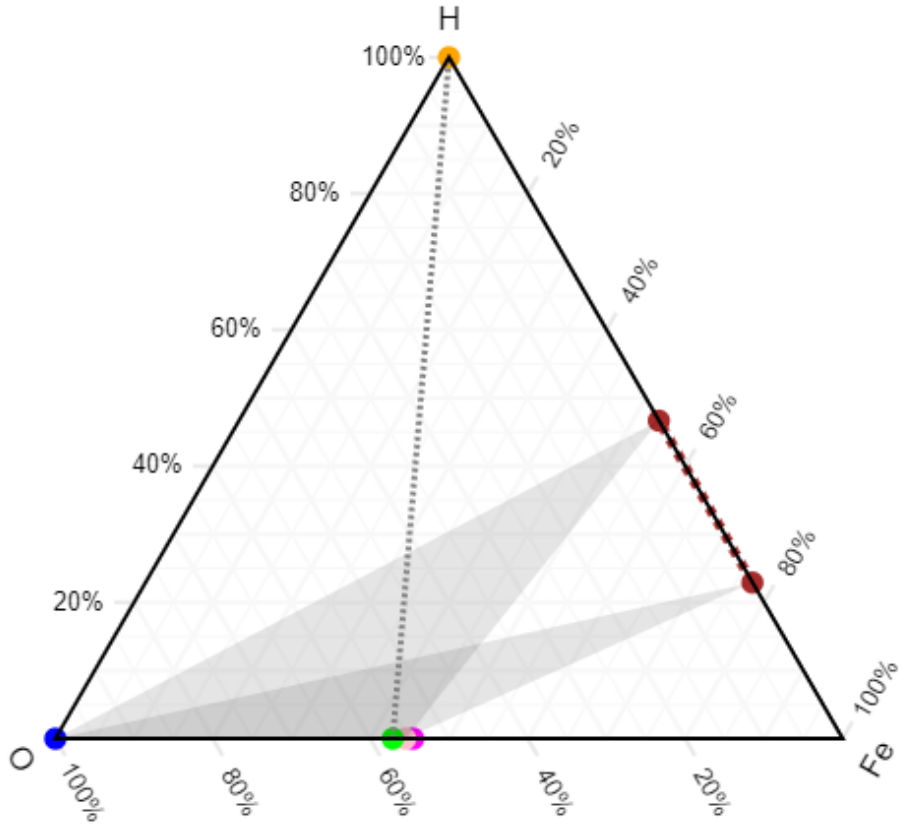

Figure 4.4: Ternary Diagram for Fe_3O_4 in Ar + H_2. Circles are of Phases Fe_3O_4: Bight-Green, Fe_4O_5: Light-Pink, Fe_5O_6: Magenta, and O_2: Blue, FeH: Brown, and H_2: Orange. The Brown Dashed Line Connect the Minimum and Maximum Calculated Hydrogen Amounts in FeH (Table 4.1). The Grey Dotted Line Connects the Reactants; Fe_3O_4 and H_2. The Grey Areas Connect the Stable Products; Fe_4O_5, FeH_x, and O_2.

4.2 IRON HYDRIDE (FeH) HYDROGEN AMOUNTS

Iron hyrdride (FeH) contains metallic iron (Fe^0). FeH (dhcp) was identified in Ar + H_2 experiments for α-Fe_2O_3 and ϵ-FeOOH, and FeH (fcc) was identified in Ar + H_2 experiments for Fe_3O_4. Neither FeH (dhcp) or FeH (fcc) were identified in the ϵ-FeOOH experiment with hydrogen-free Ar pressure medium, nor were these iron hydrides seen in the hydrogen-free pressure mediums of Ono *et al.* (2004) and Ricolleau and Fei (2016). This shows that the hydrogen in the Ar + H_2 pressure

medium mixture is sufficiently reducing to produce Fe^0.

To calculate the amount of hydrogen in FeH (dhcp) and FeH (fcc), Eq. 4.10 was used (Ikuta *et al.*, 2019). V_{FeH} is the unit-cell volume of FeH with volume measured at high pressure using XRD, V_{Fe} is the unit-cell volume of metallic Fe at high pressure (Dewaele *et al.*, 2006; Pépin *et al.*, 2014), and δV_H is expansion of the unit-cell volume by incorporating hydrogen in metallic iron to form FeH (fcc) (Ikuta *et al.*, 2019) and FeH (dhcp) (Machida *et al.*, 2019). The x is the amount of hydrogen within FeH.

$$x = \frac{V_{FeH} - V_{Fe}}{\delta V_H} \tag{4.10}$$

The calculated hydrogen amounts (x) show correlation with pressure only for the FeH (fcc) identified for the Fe_3O_4 staring material. The calculated x show an increase of H with an increase in pressure. However, this one instance does not prove that the H amount in FeH increase with pressure since the H amount in FeH (dhcp) identified in the α-Fe_2O_3 and ϵ-FeOOH do not consistently increase with pressure increase. The correlation with the H amount in FeH (fcc) for Fe_3O_4 may be coincidental since there were only three pressures to make calculations on.

Iron hydride was identified using *in situ* XRD for all three starting materials of α-Fe_2O_3, ϵ-FeOOH, and Fe_3O_4 in Ar + H_2 pressure medium. However, iron hydride was not the only phase identified in these experiments and all three of the experiments showed iron in mixed valence state of Fe^{3+}, Fe^{2+}, and Fe^0. This shows that Fe^0 can coexist with Fe^{3+} and Fe^{2+}. The mixed oxidation state could be related to the charge disproportionation reaction 1.1 (Frost *et al.*, 2004; McCammon, 2005), and shows that both pressure and redox state affects the oxidation state of iron.

Also, the production of FeH (dhcp) in the α-Fe_2O_3 experiment shows that hydrogen participates in the chemical reaction even when hydrogen is included as a diluted form within the Ar + H_2 pressure medium at 3vol%.

(a)

H_x amount in FeH (dhcp)

Sample	Spot #	P	T	δV_H	V_{Fe}	V_{FeH}	x
		(GPa)	(K)		($Å^3$)		
Fe_2O_3	1	36.5	1800	2.48	9.6	10.651	0.4236
Fe_2O_3	2	48	1900	2.48	9.2	10.867	0.6722
Fe_2O_3	3	61	1900	2.48	9	10.226	0.4942
FeOOH	1	30	1850	2.48	9.8	10.874	0.4329
FeOOH	2	40	1850	2.48	9.5	10.554	0.4251
FeOOH	3	46	1850	2.48	9.4	10.386	0.3974
FeOOH	4	50	1900	2.48	9.2	10.281	0.4358
FeOOH	5	60	1900	2.48	9	10.159	0.4671
FeOOH	6	65	2400	2.48	8.9	10.314	0.5703

(b)

H_x amount in FeH (fcc)

Sample	Spot #	P	T	δV_H	V_{Fe}	V_{FeH}	x
		(GPa)	(K)		($Å^3$)		
Fe_3O_4	1	26	1800	2.22	10.4	10.677	0.1249
Fe_3O_4	2	30	1800	2.22	9.8	10.435	0.2861
Fe_3O_4	3	35	1800	2.22	9.6	11.16	0.7028

Table 4.1: The Calculated Values for the Amount of Hydrogen (H_x) in Both dhcp and fcc Phases Identified from XRD Analysis Using the δV_H from Ikuta *et al.* (2019) for fcc and Machida *et al.* (2019) for dhcp. V_{Fe} is from Dewaele *et al.* (2006). For V_{FeH}, the Tweak Unit-Cell Volume was Used. Equation 4.10 was Used to Calculate H_x (a) Shows the FeH_x Hydrogen Amount (x) for dhcp. This Phase was Identified in all of the Heating Spots for the Starting materials α-Fe_2O_3 and ϵ-FeOOH. (b) Shows the FeH_x Hydrogen Amount (x) for fcc. This Phase was identified in all of the heating Spots for the Starting Material Fe_3O_4.

Chapter 5

CONCLUSION

Despite the importance, redox control for lower mantle mineralogy remains challenging in laser-heated diamond anvil cell (LHDAC) (McCammon, 2005; Frost and McCammon, 2008; Bindi *et al.*, 2020). Although some attempts have been made in recent experiments (Shim *et al.*, 2017), no direct control of redox and experimental confirmation for reducing conditions have been made. In order to develop redox control in LHDAC, in this thesis the method of using an Ar + H_2 medium was tested.

I conducted experiments on α-Fe_2O_3 (hematite), ϵ-FeOOH ($CaCl_2$-type), and Fe_3O_4 (magnetite) using an Ar + H_2 medium from 26-65 GPa and 1400-1900 K. Experiments on ϵ-FeOOH were also conducted using an Ar medium for direct comparison between a hydrogen-free medium and the hydrogen-bearing medium. Literature on α-Fe_2O_3 (Ono *et al.*, 2004) and Fe_3O_4 (Ricolleau and Fei, 2016) in a hydrogen-free medium were directly compared with the data in this study.

The XRD from this study of α-Fe_2O_3 in Ar + H_2 medium from 36.5-61 GPa and 1800-1900 K showed the phases Fe_5O_7, Fe_5O_6, FeH (dhcp), and ϵ-FeOOH. These products contain Fe^{3+}, Fe^{2+}, and Fe^0 (Table 3.1). For example, Fe^{3+} and Fe^{2+} mixed valence states in Fe_5O_6 (Fe^{3+}:Fe^{2+} = 2:3) and Fe_5O_7 (Fe^{3+}:Fe^{2+} = 4:1) (Table 1.1). FeH has the most reduced form, Fe^0. Literature on α-Fe_2O_3 in the hydrogen-free media of Ar and NaCl from 12.8-68.2 GPa and 1300-2500 K showed the phases α-Fe_2O_3, perovskite type (ζ-Fe_2O_3), and post-perovskite type (η-Fe_2O_3) (Ono *et al.*, 2004). These phases are all ferric iron phases. Comparing my results with Ono *et al.* (2004) suggests that Ar + H_2 medium provides reducing conditions based on the reduced iron oxide phases identified in XRD.

The XRD for the ϵ-FeOOH in Ar + H_2 medium from 30-65 GPa and 1850-1900 K showed the phases Fe_5O_7, FeH (dhcp), ϵ-FeOOH, and η-Fe_2O_3. These products contain Fe^{3+}, Fe^{2+}, and Fe^0 (Table 3.2). For example, Fe^{3+} and Fe^{2+} mixed valence states in Fe_5O_7 (Fe^{3+}:Fe^{2+} = 4:1) (Table 1.1). The XRD for ϵ-FeOOH in Ar medium from 30-52 GPa and 1400-1900 K showed the phases ι-Fe_2O_3 and ϵ-FeOOH. These phases are all ferric iron phases. Comparing my Ar + H_2 and Ar results suggests that Ar + H_2 medium promotes reducing conditions based on the reduced iron oxide phases identified in XRD.

The XRD for the Fe_3O_4 experiment showed the phases Fe_4O_5, Fe_5O_6, and FeH (fcc). These products contain Fe^{3+}, Fe^{2+}, and Fe^0 (Table 3.3). For example, Fe^{3+} and Fe^{2+} mixed valence states in Fe_4O_5 (Fe^{3+}:Fe^{2+} = 2:2) and Fe_5O_6 (Fe^{3+}:Fe^{2+} = 2:3) (Table 1.1). Literature on Fe_3O_4 in the hydrogen-free mediums of Ar and Ne from 26-64 GPa and 1300-2300 K showed the phase h-Fe_3O_4 (Ricolleau and Fei, 2016). This phase has the same iron valence state ratio as the starting material. Comparing my Ar + H_2 and Ar results of Ricolleau and Fei (2016) suggests that Ar + H_2 medium promotes reducing conditions based on the reduced iron oxide phases identified in XRD.

In this study all three starting materials of α-Fe_2O_3, ϵ-FeOOH, and Fe_3O_4 in the Ar + H_2 medium suggest that the hydrogen in the Ar + H_2 medium promotes reducing conditions. While the results presented in this thesis clearly demonstrate the potential of using an Ar + H_2 medium for redox control, there are areas I can suggest for further improvement of the technique for laser-heated diamond-anvil cell. This Ar + H_2 medium includes a 3vol% of H_2. Future work to continue the study of oxygen fugacity control within the DAC includes varying the amount of H_2 within the medium. Increasing and decreasing the H_2 amount in the medium mixture would allow for better understanding of H_2 as a reducing agent. If the study of iron oxides or

iron hydroxides in an Ar + H_2 medium is to be continued to be studied there should be consideration for the participation of hydrogen within the reaction (Eq. 4.2, 4.3, and 4.4). I found that hydrogen does participate in the reactions. This method may not provide conditions that are truly buffering. Therefore, more developments are required to prevent hydrogen from directly reacting with the sample in the case that this technique is further developed for redox experiments. If the participation of hydrogen is of interest to experiments, the incorporation of H_2 in nominally anhydrous minerals in the lower mantle under sufficient reducing conditions could be done with the current technique which will provide an important opportunity to experimentally study the subject.

It was found consistently that the diffraction rings are highly spotty during and after laser-heating. Such spottiness indicates growth of a few micron-sized crystals during laser heating. Therefore, multi-crystal type of diffraction patterns were collected rather than powder diffraction patterns. In fact, many of the iron oxide phases we found in our study were discovered through multi-crystal diffraction methods (Lavina *et al.*, 2011; Lavina and Meng, 2015; Bykova, 2015; Bykova *et al.*, 2016; Myhill *et al.*, 2016). In the future, multi-crystal type XRD measurements would be important for accurate identification of the phases. On the other hand, multi-crystal type diffraction patterns prevented us from obtaining phase fractions through Rietveld analysis. The phase fractions are particularly important to quantify the $Fe^{3+}/\Sigma Fe$ in the synthesis products. Therefore, future study should develop methods to reduce the re-crystallization of iron oxide during laser heating or oscillation of diamond-anvil cells for improve continuity of diffraction rings.

The redox conditions of the synthesis products in laser-heated diamond-anvil cell can be studied using electron energy loss spectroscopy (EELS) measurements on the recovered samples (Shim *et al.*, 2017). This would be a powerful method for the type

of experiments we presented here. In the synthesis products, we found iron oxides with varying O/Fe ratios and metallic iron. Therefore, energy-dispersive X-ray spectroscopy (EDX) measurements in scanning electron microscope (SEM) or electron probe microanalyzer (EPMA) could provide valuable information. Measurements using EPMA were attempted in this research. Unfortunately, it was found that the samples synthesized under soft Ar + H_2 medium is mechanically weak. Samples can break easily during recovery and they can escape from the sample chamber during unloading because of violent transition from solid to liquid/gas of the Ar + H_2 medium. Therefore, future studies should address these technical challenges to enable direct chemical analysis of the recovered synthesis products using TEM, SEM, and EPMA.

Over the decades, many efforts have been made in mineral physics to improve pressure and temperature measurements in the diamond anvil cell (Shim *et al.*, 2002; Ye *et al.*, 2017; Fei *et al.*, 2007; Kulka *et al.*, 2020). Efforts towards improving measurements of the physical properties of a sample have also been made (Marquardt and Marquardt, 2012; Schulze *et al.*, 2017). Despite the importance redox conditions may have, there has not been much technical developments made towards redox control. Studies that would be interesting to conduct include the study of possible mantle compositions within an Ar + H_2 medium. The charge disproportionation reaction has been important for the redox conditions of the lower mantle (Frost *et al.*, 2004; McCammon, 2005). The argument has been that such reaction would be independent of redox conditions. However, Ar + H_2 will ensure reducing conditions. It would be important to examine if charge disproportionation reaction in bridgmanite can occur even under very reducing conditions with an Ar + H_2 medium. However, efforts for understand the charge disproportionation reaction in bridgmanite have been made through the use of a redox buffer, not a pressure medium (Kurnosov *et al.*, 2017).

Recently, FeO_2H_x has been discussed for possible water carrier in the deep man-

tle (Hu *et al.*, 2016; Nishi *et al.*, 2017). It has been argued that even under reducing conditions extra oxygen can exist in the lower mantle (McCammon, 2005; Hu *et al.*, 2016). However, none of these experiments have included redox control or sufficiently reducing conditions found in the lower mantle. In fact, some of the samples were synthesized with an H_2O medium or O_2 medium, which can be oxidizing, and therefore, not related to the conditions expected for the lower mantle. Though redox conditions are not the only important condition to consider within the lower mantle (410-2900 km) (McCammon, 2005), being able to control oxygen fugacity can allow for experimental conditions more similar to the complex conditions of the lower mantle.

REFERENCES

Bindi, L., S.-H. Shim, T. G. Sharp and X. Xie, "Evidence for the charge disproportionation of iron in extraterrestrial bridgmanite", Science advances **6**, 2, eaay7893 (2020).

Bykova, E., *Single-crystal X-ray diffraction at extreme conditions in mineral physics and material sciences*, Ph.D. thesis (2015).

Bykova, E., L. Dubrovinsky, N. Dubrovinskaia, M. Bykov, C. McCammon, S. V. Ovsyannikov, H.-P. Liermann, I. Kupenko, A. I. Chumakov, R. Rüffer *et al.*, "Structural complexity of simple fe 2 o 3 at high pressures and temperatures", Nature communications **7**, 1, 1–6 (2016).

Dewaele, A., P. Loubeyre, F. Occelli, M. Mezouar, P. I. Dorogokupets and M. Torrent, "Quasihydrostatic equation of state of iron above 2 mbar", Physical Review Letters **97**, 21, 215504 (2006).

Dobson, D. P. and J. P. Brodholt, "Subducted banded iron formations as a source of ultralow-velocity zones at the core–mantle boundary", Nature **434**, 7031, 371–374 (2005).

Dorogokupets, P. I., T. S. Sokolova, B. S. Danilov and K. D. Litasov, "Near-absolute equations of state of diamond, ag, al, au, cu, mo, nb, pt, ta, and w for quasi-hydrostatic conditions", Geodynamics & Tectonophysics **3**, 2, 129–166 (2015).

Errandonea, D., R. Boehler, S. Japel, M. Mezouar and L. Benedetti, "Structural transformation of compressed solid ar: An x-ray diffraction study to 114 gpa", Physical Review B **73**, 9, 092106 (2006).

Fei, Y., A. Ricolleau, M. Frank, K. Mibe, G. Shen and V. Prakapenka, "Toward an internally consistent pressure scale", Proceedings of the National Academy of Sciences **104**, 22, 9182–9186 (2007).

Frost, B. R., *Oxide minerals: petrologic and magnetic significance*, vol. 25 (Walter de Gruyter GmbH & Co KG, 1991).

Frost, D. J., C. Liebske, F. Langenhorst, C. A. McCammon, R. G. Trønnes and D. C. Rubie, "Experimental evidence for the existence of iron-rich metal in the earth's lower mantle", Nature **428**, 6981, 409–412 (2004).

Frost, D. J. and C. A. McCammon, "The redox state of earth's mantle", Annu. Rev. Earth Planet. Sci. **36**, 389–420 (2008).

Hu, Q., D. Y. Kim, W. Yang, L. Yang, Y. Meng, L. Zhang and H.-K. Mao, "Feo 2 and feooh under deep lower-mantle conditions and earth's oxygen–hydrogen cycles", Nature **534**, 7606, 241–244 (2016).

Ikuta, D., E. Ohtani, A. Sano-Furukawa, Y. Shibazaki, H. Terasaki, L. Yuan and T. Hattori, "Interstitial hydrogen atoms in face-centered cubic iron in the earth's core", Scientific reports **9**, 1, 1–8 (2019).

Kulka, B. L., J. D. Dolinschi, K. D. Leinenweber, V. B. Prakapenka and S.-H. Shim, "The bridgmanite–akimotoite–majorite triple point determined in large volume press and laser-heated diamond anvil cell", Minerals **10**, 1, 67 (2020).

Kurnosov, A., H. Marquardt, D. J. Frost, T. B. Ballaran and L. Ziberna, "Evidence for a fe 3+-rich pyrolitic lower mantle from (al, fe)-bearing bridgmanite elasticity data", Nature **543**, 7646, 543–546 (2017).

Lavina, B., P. Dera, E. Kim, Y. Meng, R. T. Downs, P. F. Weck, S. R. Sutton and Y. Zhao, "Discovery of the recoverable high-pressure iron oxide fe4o5", Proceedings of the National Academy of Sciences **108**, 42, 17281–17285 (2011).

Lavina, B. and Y. Meng, "Unraveling the complexity of iron oxides at high pressure and temperature: Synthesis of fe5o6", Science Advances **1**, 5, e1400260 (2015).

Machida, A., H. Saitoh, T. Hattori, A. Sano-Furukawa, K.-i. Funakoshi, T. Sato, S.-i. Orimo and K. Aoki, "Hexagonal close-packed iron hydride behind the conventional phase diagram", Scientific reports **9**, 1, 1–9 (2019).

Marquardt, H. and K. Marquardt, "Focused ion beam preparation and characterization of single-crystal samples for high-pressure experiments in the diamond-anvil cell", American Mineralogist **97**, 2-3, 299–304 (2012).

McCammon, C., "The paradox of mantle redox", Science **308**, 5723, 807–808 (2005).

Myhill, R., D. O. Ojwang, L. Ziberna, D. J. Frost, T. B. Ballaran and N. Miyajima, "On the ptfo2 stability of fe4o5, fe5o6 and fe4o5-rich solid solutions", Contributions to Mineralogy and Petrology **171**, 5, 51 (2016).

Nishi, M., Y. Kuwayama, J. Tsuchiya and T. Tsuchiya, "The pyrite-type high-pressure form of feooh", Nature **547**, 7662, 205–208 (2017).

Ono, S., T. Kikegawa and Y. Ohishi, "High-pressure phase transition of hematite, fe2o3", Journal of Physics and Chemistry of Solids **65**, 8-9, 1527–1530 (2004).

Pépin, C. M., A. Dewaele, G. Geneste, P. Loubeyre and M. Mezouar, "New iron hydrides under high pressure", Physical review letters **113**, 26, 265504 (2014).

Prescher, C. and V. B. Prakapenka, "Dioptas: a program for reduction of two-dimensional x-ray diffraction data and data exploration", High Pressure Research **35**, 3, 223–230 (2015).

Ricolleau, A. and Y. Fei, "Equation of state of the high-pressure fe3o4 phase and a new structural transition at 70 gpa", American Mineralogist **101**, 3, 719–725 (2016).

Righter, K., C. D. Herd and A. Boujibar, "Redox processes in early earth accretion and in terrestrial bodies", Elements: An International Magazine of Mineralogy, Geochemistry, and Petrology **16**, 3, 161–166 (2020).

Schulze, K., J. Buchen, K. Marquardt and H. Marquardt, "Multi-sample loading technique for comparative physical property measurements in the diamond-anvil cell", High Pressure Research **37**, 2, 159–169 (2017).

Shim, S.-H., "Peakpo - a python software for x-ray diffraction analysis at high pressure and high temperature", (2017).

Shim, S.-H., A. Bengtson, D. Morgan, W. Sturhahn, K. Catalli, J. Zhao, M. Lerche and V. Prakapenka, "Electronic and magnetic structures of the postperovskite-type fe2o3 and implications for planetary magnetic records and deep interiors", Proceedings of the National Academy of Sciences **106**, 14, 5508–5512 (2009).

Shim, S.-H., T. S. Duffy and K. Takemura, "Equation of state of gold and its application to the phase boundaries near 660 km depth in earth's mantle", Earth and Planetary Science Letters **203**, 2, 729–739 (2002).

Shim, S.-H., B. Grocholski, Y. Ye, E. E. Alp, S. Xu, D. Morgan, Y. Meng and V. B. Prakapenka, "Stability of ferrous-iron-rich bridgmanite under reducing midmantle conditions", Proceedings of the National Academy of Sciences **114**, 25, 6468–6473 (2017).

Stagno, V. and Y. Fei, "The redox boundaries of earth's interior", Elements: An International Magazine of Mineralogy, Geochemistry, and Petrology **16**, 3, 167–172 (2020).

Thomas, E. L., "Crystal growth and the search for highly correlated ternary intermetallic antimonides and stannides", (2006).

Tuček, J., L. Machala, S. Ono, A. Namai, M. Yoshikiyo, K. Imoto, H. Tokoro, S.-i. Ohkoshi and R. Zbořil, "Zeta-fe 2 o 3–a new stable polymorph in iron (iii) oxide family", Scientific reports **5**, 1, 1–11 (2015).

Wood, B. J., M. J. Walter and J. Wade, "Accretion of the earth and segregation of its core", Nature **441**, 7095, 825–833 (2006).

Ye, Y., V. Prakapenka, Y. Meng and S.-H. Shim, "Intercomparison of the gold, platinum, and mgo pressure scales up to 140 gpa and 2500 k", Journal of Geophysical Research: Solid Earth **122**, 5, 3450–3464 (2017).